Using hydrogeochemistry to understand inter-aquifer mixing in the on-shore part of the Gippsland Basin, southeast Australia

H. Hofmann *, Ian Cartwright

School of Geosciences, Monash University, Wellington Road, Clayton, Victoria 3800, Australia
National Centre for Groundwater Research and Training, Flinders University, Adelaide, SA 5001, Australia

ABSTRACT

Groundwater in the Latrobe Valley in the Gippsland Basin of southeast Australia is important for domestic, agricultural and industrial uses. This sedimentary basin contains a number of aquifers that are used for water supply, dewatered for open pit coal mining, and which are potentially influenced by off-shore oil and gas production. Major ion chemistry together with stable and Sr isotope data imply that the main hydrogeochemical processes are evapotranspiration with minor silicate and carbonate weathering; methanogenesis and SO_4 reduction in reduced groundwater associated with coal deposits have also occurred. Groundwater has estimated ^{14}C ages of up to 36 ka and is largely ^{3}H free. Carbon-14 ages are irregularly distributed and poorly correlated with depth and distance from the basin margins. The observations that the geochemistry of groundwater in aquifers with different mineralogies are similar and the distribution of ^{14}C ages is irregular implies that the aquifers are hydraulically connected and horizontal as well as vertical inter-aquifer mixing occurs. The connection of shallow and deeper aquifers poses a risk for the groundwater resources in Gippsland as contaminants can migrate across aquifers and dewatering of shallow units may impact deeper parts of the groundwater system.

© 2013 Elsevier Ltd. All rights reserved.

1. Introduction

Groundwater in sedimentary basins is an essential resource for both healthy ecosystems as well as for domestic, agricultural and industrial use. Given that the global demand for groundwater is increasing, understanding groundwater systems is critical for sustainable management of water resources. The most utilized groundwater resources occur in sedimentary basins. Because of the continuity of stratigraphy, foreland and intra-mountain basins host the largest groundwater flow systems (Fogg, 1986; Downing et al., 1987; Tóth, 1995; Mahlknecht et al., 2004; Ma et al., 2005; Ross et al., 2005) and are also often extensively exploited for petroleum and mineral deposits (Garven, 1995). Sustainable management of the groundwater resources in these large complex multi-aquifer systems requires a detailed understanding of recharge distribution and rates, groundwater residence times, as well as groundwater flow paths to avoid overexploitation or cross-aquifer contamination.

Stratigraphy, topography, heterogeneities in hydraulic conductivity, and basin geometry are the primary factors controlling the patterns of groundwater flow (Freeze, 1974; Jencso and McGlynn, 2011). Groundwater flow in basins containing heterogeneous strati-

graphic sequences where aquitards are locally absent or that are disrupted by fault systems or folding may be complex (Carrillo-Rivera et al., 2007; Ayraud et al., 2008; Cartwright et al., 2010). Horizontal groundwater flow parallel to the stratigraphy is fairly straightforward to determine using hydraulic head data and hydraulic conductivities. Vertical groundwater flow within and between formations, however, is more difficult to define due to higher aquifer anisotropy in a vertical direction than in the direction of the bedding. Furthermore, vertical hydraulic conductivities are less commonly measured (Sayed et al., 1992). Where aquifers are separated by aquitards vertical flow may be limited. By contrast, where aquitards are locally absent or are cut by fracture systems, significant inter-aquifer flow may occur. Documenting inter-aquifer flow is important. If groundwater flow is largely parallel to stratigraphy, deeper groundwater may be protected from near surface contamination; likewise, shallow groundwater and connected surface water systems may be isolated from the impacts of pumping of deeper aquifers. By contrast, significant inter-aquifer flow may compromise both the quality and quantity of surface water and groundwater.

Groundwater geochemistry is a valuable tool to determine inter-aquifer mixing and flow regimes (Dogramaci and Herczeg, 2002; Raiber et al., 2009; Edmunds, 2009; Cartwright et al., 2010). Unlike hydraulic heads that may be perturbed due to pumping or changes in recharge rates following land use changes, groundwater geochemistry reflects the long-term flow in aquifer systems. Especially in aquifer systems with distinct mineralogical

* Corresponding author at: School of Geosciences, Monash University, Wellington Road, Clayton, Victoria 3800, Australia. Tel.: +61 3 990 55786; fax: +61 3 990 54903.
E-mail address: harald.hofmann@monash.edu (H. Hofmann).

differences, major ion chemistry, $\delta^{13}C$ values, and $^{87}Sr/^{86}Sr$ ratios can indicate mixing in between aquifer units (Dogramaci and Herczeg, 2002; Cartwright et al., in press). If the mineralogy of the aquifers is similar, environmental stable and radiogenic isotopes can be used to identify inter-aquifer mixing (Fontes, 1983; Zuber et al., 2005; Cartwright et al., 2010). Tritium has been used extensively to date groundwater <60 a and is useful for identifying recharge zones and short-timescale leakage of surface water into deeper aquifers. ^{14}C is suitable for dating groundwater with an age of up to ~30 ka (Maloszewski and Zuber, 1991; Mazor, 2004). In simple flow systems, ^{14}C ages increase from the basin margins towards the centre of the basin and also increase with depth; by contrast, if there is significant inter-aquifer mixing, ^{14}C ages may not show such a regular distribution.

This study focuses on the Latrobe Valley in the on-shore part of the Gippsland Basin, Victoria, Australia (Fig. 1). The Gippsland Basin is a large coastal sedimentary basin with important petroleum, gas and coal deposits. Dewatering of open-pit coal mines and oil and gas production extract considerable volumes of groundwater from the basin; additionally, the basin also provides water for one of Victoria's most significant agricultural areas and for domestic supply. Approximately 95,100 ML of groundwater was extracted in the Gippsland Basin in 2007 (Department of Sustainability and Environment, 2009). Because the base of the coal pits in the Latrobe Valley is 60–80 m below the natural surface (Holdgate et al., 2000), the water table in the vicinities of the coal pits has been lowered by approximately 100 m (Thompson, 1986). Dewatering of mine sites, off-shore oil and gas production and water extraction for irrigation have caused complex changes in groundwater flow patterns and over the last 30 a head levels have declined in most aquifer units in the Gippsland Basin (Gibson-Poole et al., 2008; Varma and Michael, 2011) (Fig. 3). Estimates

of recharge rates for the Latrobe Valley based on a combination of flow calculations, Cl^- mass balance, and the infiltration capacities of the soils are 30–67 M m^3/a (Walker and Mollica, 1990; Nahm, 2002; Schaeffer, 2008; Varma and Michael, 2010).

Despite the economic importance, the extensive water use and the documented decline in head levels there have been few published studies on the hydrogeology of the Gippsland Basin. Gibson-Poole et al. (2008) studied the off-shore part of the basin for possible CO_2 storage capacities, Varma and Michael (2010) modelled the impact of off-shore oil production on groundwater drawdown, and Schaeffer, 2008 developed a regional groundwater model. These studies concluded that flow patterns within the basin have changed drastically since the beginning of mine dewatering and oil and gas exploitation (Figs. 2 and 3). Despite these studies, little is known about inter-aquifer connectivity and groundwater residence times. Resolving these issues is critical to assessing the sustainable use of groundwater in this region.

This study uses a combination of hydrological information, major ion geochemistry, stable isotopes, $^{87}Sr/^{86}Sr$, and radiogenic isotopes (^3H and ^{14}C) to develop a conceptual hydrological model of the Latrobe Valley in the on-shore part of the Gippsland Basin, in particular, to constrain the long-term groundwater flow patterns and assess inter-aquifer mixing. The results of this study will enable a better management of the water resources in a region where there are competing demands for water use for resource, rural and domestic use.

1.1. Geographical, geological and hydrogeological overview

The Gippsland Basin is a coastal sedimentary basin in the SE of Victoria with an area of approximately 42,750 km^2 (Fig. 1). It is divided into off-shore (~35,200 km^2) and on-shore parts
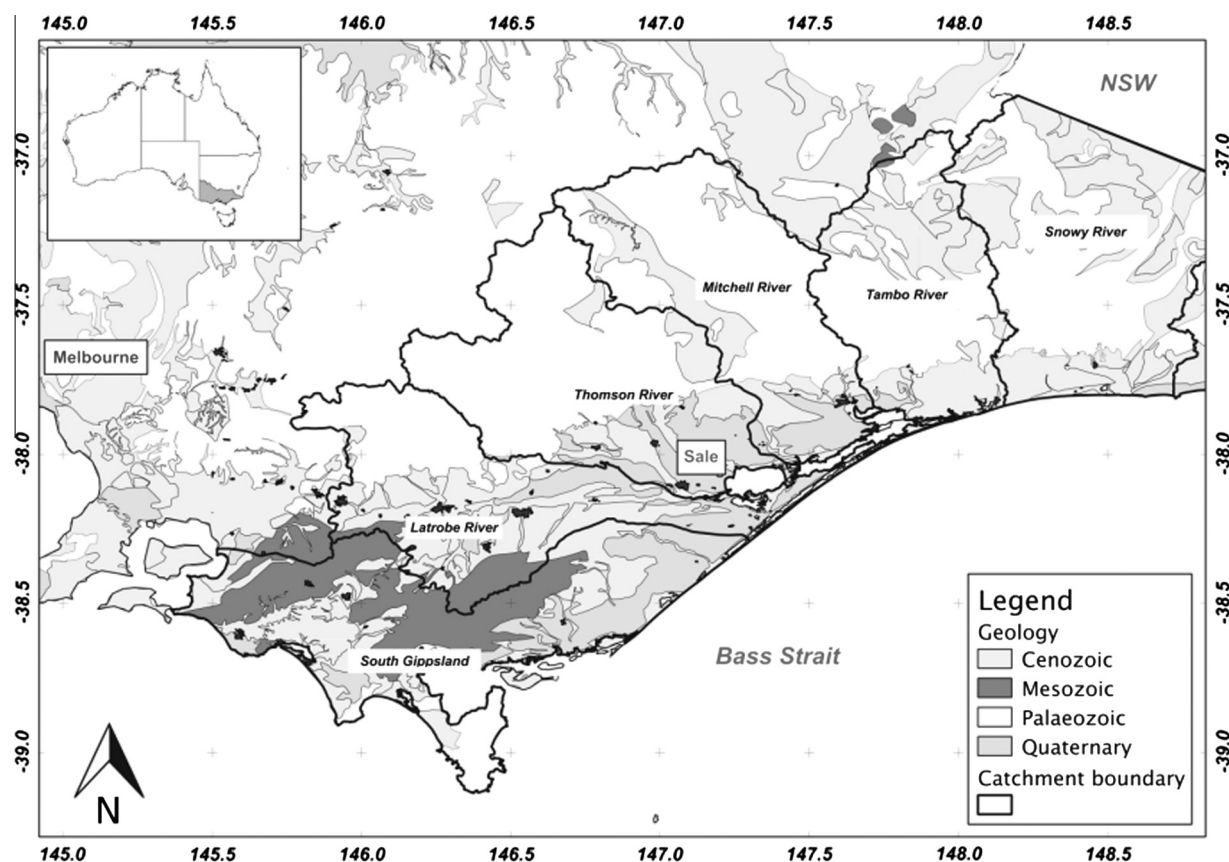

**Fig. 1.** Geological map of the Gippsland Basin and its sub-basins.

(∼7500 km²). The latter extends from Warragul, approximately 100 km east of Melbourne, to the eastern tip of Victoria at Mallacoota. The basin is bound by the Australian Alpine Ranges to the north and by the Strzelecki and Hoddle Ranges to the SW. The mountain regions are generally covered with native eucalypt forests and reach up to 1800 m (Australian Height Datum, AHD). The basin interior is intensively used for agriculture and has been mainly cleared of its original forest cover. Rainfall is highest in the mountains with average annual precipitation of over 1500 mm. The plains receive average annual rainfall of 600–950 mm. The Latrobe Valley is one of seven catchment areas in the Gippsland Basin (Fig. 1). It contains rich coal deposits, which are mined in the area around the cities of Moe, Morwell and Traralgon from open pits.

Geologically, the Gippsland Basin is an east–west trending structure that formed as a consequence of the break-up of Gondwana in the Mesozoic (Rahmanian et al., 1990; Willcox and Sayers, 2001) when rifting began in the Cretaceous, followed by opening of the Southern Ocean in the Eocene–Oligocene. It is bounded to the north by Palaeozoic basement of the Eastern Uplands (East Gipplsand Rise), to the west by uplifted Lower Cretaceous fault-blocks and to the SW by the Bassian Rise (O'Sullivan et al., 2000), which separates it from the Bass Basin to the west (Norvick et al., 2001). In SE Victoria the Palaeozoic basement comprises mostly Ordovician to Early Devonian low grade metamorphic sandstones, shales and turbidites of the Lachlan Fold Belt, intruded by Middle Devonian granites (Webb et al., 2011). A series of marine transgressions and regressions produced a complex sequence of
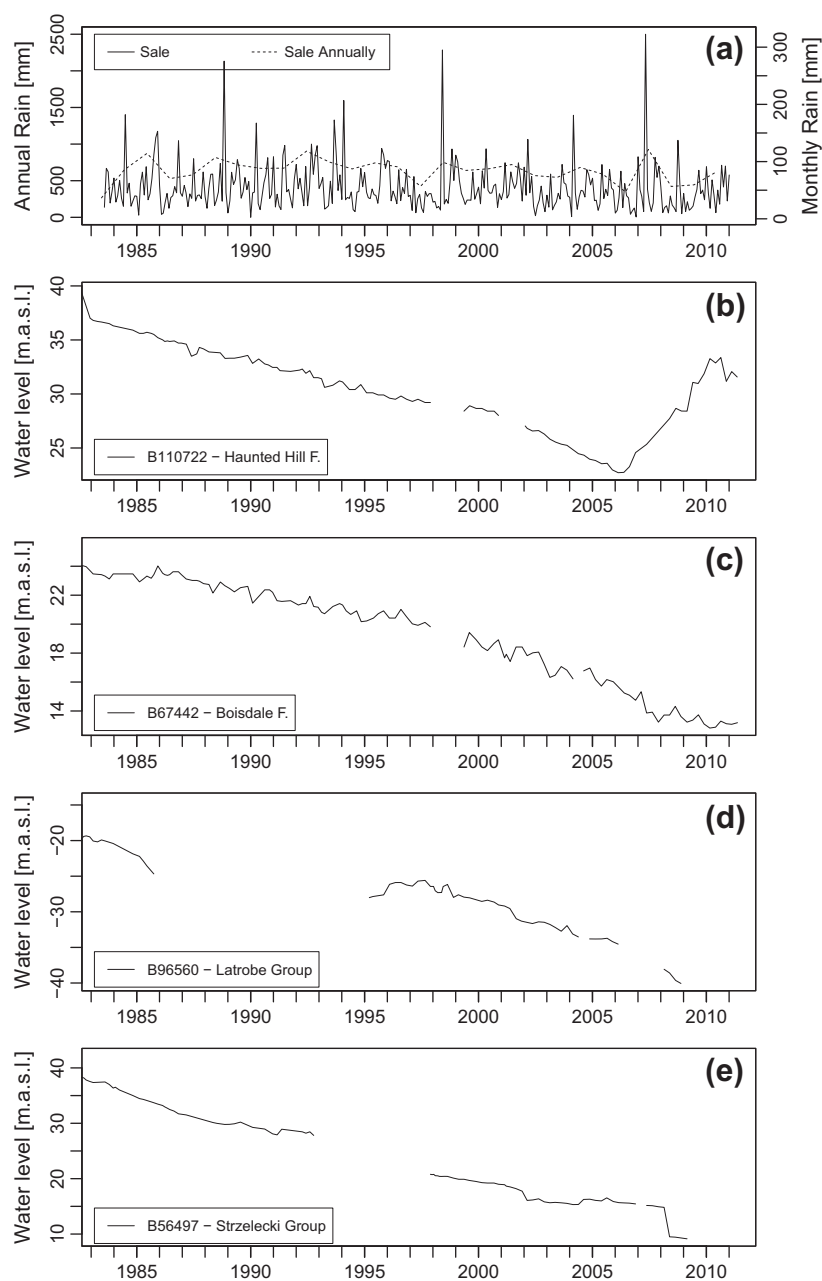
Fig. 2. Bore hydrographs of selected bores in the Latrobe Valley from 1983 to today. (a) Annual and monthly rainfall for the weather station in Sale, Victoria (Data source Bureau of Meteorology), (b–e) falling hydrograph in the Haunted Hill Formation, the Boisdale Formation, the Latrobe Group and the Stzelecki Formation; Data source, Victorian Water Warehouse (2011).
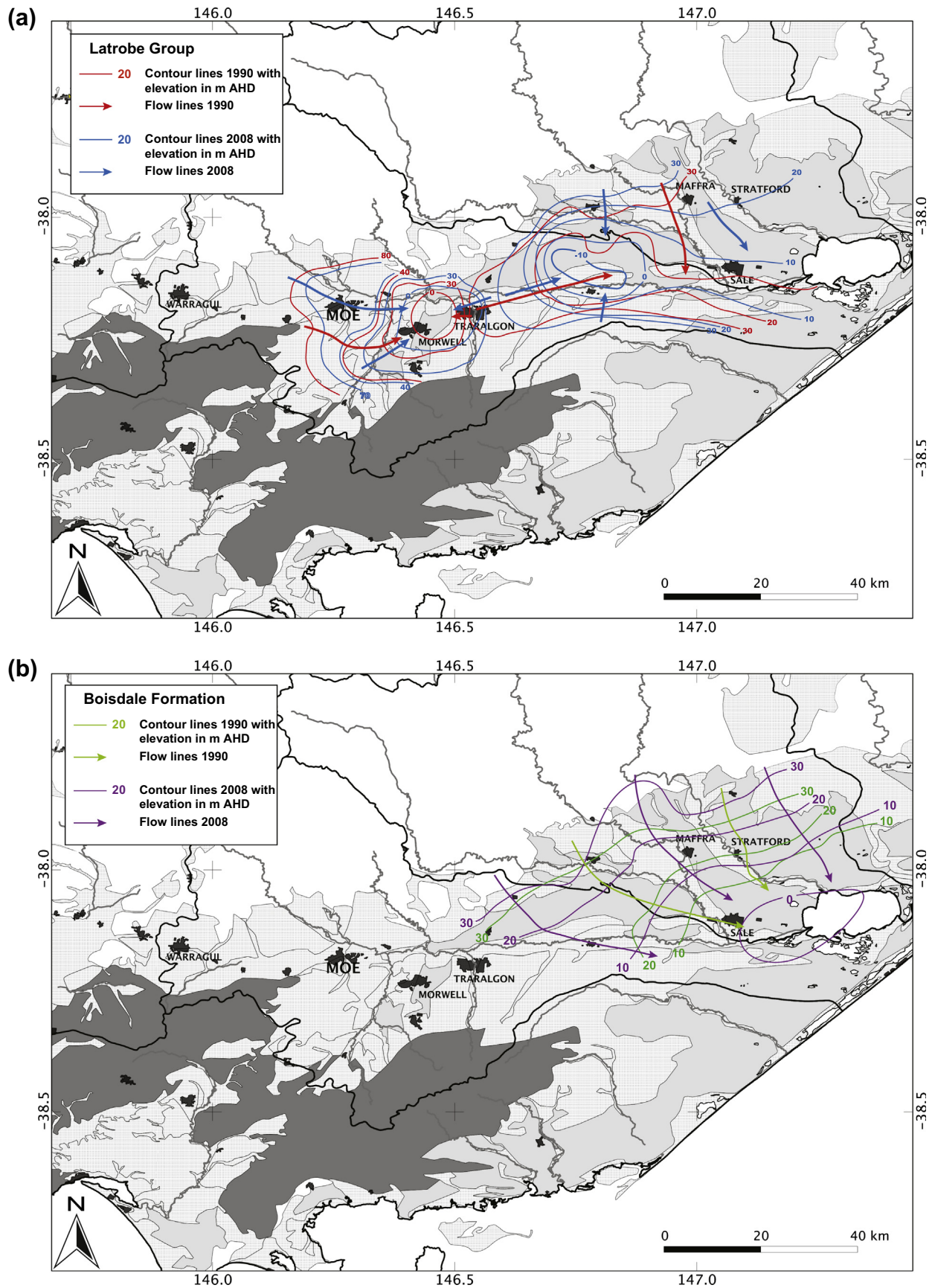
Fig. 3. (a) Approximated groundwater flow pattern in the Latrobe Valley for the Latrobe Group aquifer in 1990 (red) and 2008 (blue). (b) Approximated groundwater flow pattern for the Boisdale Group in the Latrobe Valley and the Thompson Catchment in 1990 (green) and 2008 (purple). (For interpretation of the references to colour in this figure legend, the reader is referred to the web version of this article.)

alternating terrestrial and marine sediments in the basin after the Cretaceous.

The Palaeozoic metasediments and granites host minor groundwater flow in fractures; however, bore yields are generally negligible in comparison with the unconsolidated younger sedimentary units (Southern Rural Water, 2009). The sedimentary aquifers within the Gippsland Basin are up to 1500 m thick onshore and thicken off-shore up to 4000 m (Gibson-Poole et al., 2006). Consolidated sandstones and shales of the Mesozoic Strzelecki Group overlie the Palaeozoic basement and form an aquitard (Tosolini et al., 1999; Varma and Michael, 2010). In the west of the basin, terrestrial sandstones, conglomerates and clays of the Childers Formation and tholeiitic and alkali basalts of the Thorpdale Volcanics constitute the major Early Tertiary aquifers (Fig. 4) that are time equivalent with the lower units of the Latrobe Valley Group. The Childers Formation is up to 40 m thick, while the Thorpdale Volcanics are up to 60 m thick (Cochrane et al., 1991) (Table 1). Hydraulic conductivities in the Thorpdale Volcanics in the Westernport Basin range from <1 to 18 m/day (Lakey and Tickell, 1981) with higher values in areas of joints, fractures, and at the interfaces between lava flows (Cochrane et al., 1991).

The Latrobe Valley Group is an amalgamation of up to 500 m thick laterally alternating sandstones, silt units, and coal seams in the centre of the basin that is divided into the Traralgon, Morwell and Yallourn Formations (Fig. 4). The Traralgon Formation is widespread in the Gippsland Basin with coal seams of up to 100 m thickness; the basal part of this unit contains up to 250 m of sand, gravel, and clay, with minor coal and olivine basalts of the Carrajung Volcanics (Douglas and Ferguson, 1988). The coal seams function as aquitards; however, in some units they are strongly jointed and are likely to be pathways of groundwater flow (Douglas and Ferguson, 1988) (Fig. 4). The younger Morwell and Yallourn Formations are predominantly coal seams interbedded with sands and clays. The sands are major aquifers with hydraulic conductivities of up to 100 m/day (Table 1).

The Balook Formation is a localised unit in the area around Rosedale that is important to the regional groundwater flow as it provides a connection between the other units (Brumley et al., 1981). The lower part consists of 200 m of fine marine sands with considerable clay content. The upper part is coarser grained with less clay. The lower part of this unit links the Morwell Formation in the west and the Lakes Entrance Formation in the east. The upper unit links to the Yallourn Formation in the west and the Gippsland Limestone in the east (Douglas and Ferguson, 1988).

The Seaspray Group in the east of the basin includes the Seaspray Sands, Gippsland Limestone, Bairnsdale Limestone, Lakes Entrance Formation, Tambo River Formation and Jemmy's Point Formation (Fig. 4). The Seaspray Sands are likely to be hydraulically connected to the Morwell Formation (Holdgate et al., 1995). They consist of fine sands with local clay lenses. The Lakes Entrance Group consists of a sequence of sands and gravels at the base, developing to finer grained marls and mudstone on the top with fine interbeds of fossiliferous sandy limestone (Gallagher et al., 2003). The Bairnsdale and Gippsland Limestones are marine marl and carbonate units with significantly lower hydraulic conductivities (2–10 m/day) (Department of Sustainability and Environment, 2010) (Table 1). They are chronologically equivalent to the Morwell and Yallourn Formations. The hydraulic properties of the Bairnsdale Formation and the Gippsland Limestones vary, with the marls forming aquitards and the rest fractured limestone aquifers (Southern Rural Water, 2009). The ~110 m thick Jemmey's Point Formation and the ~100 m thick Tambo River Formation are both marine deposits that occur in the east of the basin. The Jemmy's Point Formation consists of shelly sandy marls with calcareous
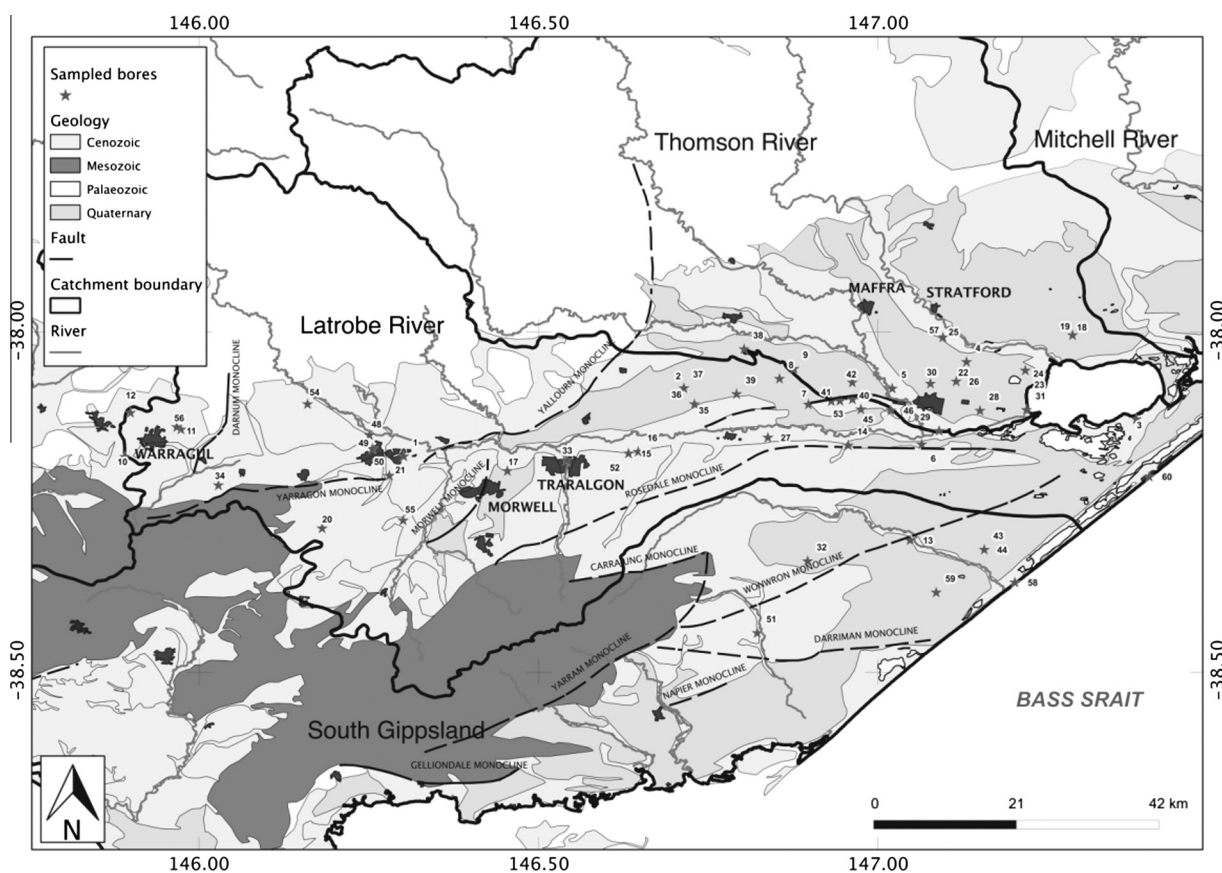

Fig. 4. Structural overview map of the Latrobe Valley and location of sample groundwater bores. Bore numbers are listed in Table 2.

Table 1
The major aquifer units in the Gippsland Basin, their approximate depth and hydraulic characteristics. Table was assembled from Cochrane et al., 1991, DSE, 2010, Southern Rural Water, 2009; Douglas and Ferguson, 1988, Brumley, 1981.

Aquifer	Age	Lithology	Conf./unconf.	Thick. (m)	Hydr. Cond. (m/d)
Quarternary alluvium	Recent	Alluvials deposited in major river valleys and consist of coarse sand and gravels	Unconf.		5–300
Sale Group	Late Miocene to Pleistocene				
Haunted Hill Formation	Plio-Pleistocene	Sands, gravels, sandy clays and clays	Outwash fan type deposits	Unconf, semi conf., conf.,	Max. 80
Boisdale Fromation	Late Miocene to Early Pliocene	Sands, gravels, clays, coal and also middle Tertiary basalts, minor aquifer system consists of limestone and marls	Marine facies, marginal marine facies and non-marine facies	Sand aquifer confined beneath clays in upper part of formation or in overlying alluvium	50–200
Seaspray Group	Early Oligocene to Early Pliocene	Marls and limestone	Mostly confined	50–400	$<$0.1–10
(Jennmys Point F., Lakes Entrance F., Tambo River F., Yarragon F., Gippsland Limestone, etc.)		Sands, sandy clays, clays and marls	Marine facies and non-marine facies. YF with thick brown coal seams and clays occur towards the top of the sequence with sands towards the base. TV, at the eastern side of the basin, the basaltic layers are interbedded with clays, sands and coals		
Balook Formation	Early Oligocene to Late Miocene	Narrow belt of fine, clay rich sands in the lower part, coarser sands with lower clay content in the upper units	Mostly confined	250–480	Undetermined
Latrobe Valley Group	Middle Palaeocene to Late Miocene		Confined, partly unconfined	20–900	10–100
(Latrobe Valley Coal Measures, Yallourn F., Morwell F., Traralgon F., etc.)		LCM is a term for all coal bearing formation in the Latrobe Valley. Others: Lake and fluviatile deposits of sand, clay and brown coal seams, partly shoreline beach – barrier sands deposits with interbedded clays			
Thorpdale Volcanics	Late Oligocene	Basalt, basaltic clay, tuff (interbedded with Traralgon and Morwell F. sediments	Confined fractured rock	Max. 60 m	1–18
Childers Formation	Early to Late Oligocene	Sand, gravel, silt and clay	Confined sand aquifer	May–40	Undetermined
Strzelecki Group	Upper Cretaceous	Principle rocks are arkoses with mudstone lensing, sandstones, conglomerates, carbonaceous layers and coal of minor quality	Confined	Max. 745	Undetermined

Table 2
Chemical data table for the sampled groundwater in the Latrobe Valley with major ions and in situ measurement. The table includes total bore depth, dimensions of the screened section and the elevation (Formation, Site ID, Bore Depth and Screen from data from Department of Sustainability and Environment, 2010).

No.	Formation	Site ID	EC (μS/cm)	T (°C)	pH	TDS (mg/L)	Cl (mg/L)	Br (mg/L)	SO$_4$ (mg/L)	HCO$_3$ (mg/L)	CO$_2$ (mg/L)	Ca (mg/L)	Mg (mg/L)	K (mg/L)	Na (mg/L)	Sr (mg/L)	Bore Depth (m)	Screen from (m)
40	Balook Formation	105134	305	16.8	8.87	204.35	67.72	0.28	1.23	31.5	38	4.02	50.27	8.56	47.87	0.108	790.9	790
3	Boisdale Formation	50876	1905	16.8	7.98	1276.35	531.96	1.66	9.83	95.34	122	42.49	1.51	12.91	248.56	1.973	146	57
4	Boisdale Formation	52753	304	17.6	9.68	203.68	74.39	0.23	0.15	26	0	3.48	16.22	4.69	45.61	0.062	269.7	169
9	Boisdale Formation	59308	772	16.6	9.4	517.24	131.1	0.59	0.25	150.78	96	5.16	2.53	5.89	120.9	0.042	250.7	65
19	Boisdale Formation	77947	402	15.3	8.22	269.34	130.05	0.39	0.04	2.52	20	7.93	11.22	7.7	61.29	0.094	116.1	106.9
22	Boisdale Formation	86464	523	18.1	6.07	350.41	84.34	0.24	0.52	100	84	11.2	10.55	11.04	78.15	0.062	239.1	104.7
23	Boisdale Formation	86465	3570	16.7	9.07	2391.9	908.26	3.48	33.61	124.32	68	1.88	92.09	15.34	565.12	0.19	171.8	112
24	Boisdale Formation	86466	745	15.2	6.65	499.15	132.93	0.38	0.28	118.44	234	4.84	8.41	33.19	55.66	0.016	121.5	111.8
25	Boisdale Formation	86669	447	15.5	8.63	299.49	96.88	0.29	0.09	54.18	36	11.41	12.55	12.88	56.73	0.08	191.9	85.1
26	Boisdale Formation	86670	560	21.9	6.34	375.2	91.48	0.29	0.44	131	32	13.5	13.21	15.12	60.61	0.093	79.9	58.7
28	Boisdale Formation	90148	580	16.8	6.29	388.6	116.99	0.32	0.02	77.7	234	9.21	6.57	16.96	79.02	0.119	188	106
29	Boisdale Formation	90149	588	15.5	6.65	393.96	79.83	0.25	0.43	108	132	12.88		11.4	56.22	0.206	206.9	143
36	Boisdale Formation	103811	2310	27.3	10.57	1547.7	286.38	0.92	4.36	18				25.5	461.58		222	78
37	Boisdale Formation	103820	1444	16.2	10.04	967.48	66.28	0.16	24.93	244.44	0	6.38	10.17	45.87	288	0.09	192	63.5
38	Boisdale Formation	103822	1224	13.4	9.04	820.08	308.54	1.41	0.07	29.82	32	3.68	7.35	9.38	203.32	0.027	251	91
39	Boisdale Formation	105132	337	24	7.53	225.79	56.73	0.18	0.04	43	42	9.67	6.19	4.29	44.59	0.177	168	28
41	Boisdale Formation	105196	396	15.8	8.27	265.32	52.42	0.22	0.06	89.46	72	37.79	48.56	13.5	58.01	0.058	252	123.4
43	Boisdale Formation	105484	2150	15.4	6.79	1440.5	545.88	2.12	34.3	134.4	278	3.83	1.85	9.34	310.74	0.736	58.3	52.2
44	Boisdale Formation	105547	355	16.2	8.09	237.85	82.4	0.33	0.56	30.24	70	9.9	7.22	9.22	53.99	0.022	396.9	153.9
45	Boisdale Formation	105548	440	16.5	7.59	294.8	100.75	0.4	0.06	52.92	66			6.75	66.04	0.095	900.4	900.4
57	Boisdale Formation	145091	1560	16.1	11.19	1045.2	321.46	1.48	28.56	0	0	101.68	13.88	16.08	164.89	0.814	64	64
58	Boisdale Formation	145092	799	16.3	6.77	535.33	194.79	0.65	11.62	61.32	164	18.71		4.2	115.76	0.217	90	90
59	Boisdale Formation	145093	5970	22.4	5.9	3999.9	733.85	2.3	1.34	30	270	240.37	104.22	30.62	822.83	1.839	79	79
47	Childers Formation	107971	483	16.4	6.67	323.61	61.1	0.25	0.35	115.92	208	24.83	16.68	11.9	39.01	0.206	121	110.6
48	Childers Formation	107972	549	17.2	6.16	367.83	69.93	0.29	0.05	133.56	154	33.75	16.55	14.24	52.66	0.513	256.6	225.6
49	Childers Formation	107973	619	17.1	7.64	414.73	52.38	0.21	1.58	202.44	96	49.46	34.45	12.49	45.16	0.36	150	136
1	Haunted Hill	23726	140	16.1	7.81	93.8	22.01	0.08	0.22	20.58	22	3.05	1.19	5.42	17.68	0.027	20.5	14
2	Haunted Hill	45759	4720	18.5	6.93	3162.4	1298.11	3.41	95.5	117	74	7.4	112.64	21	782.13	0.154	23.5	20
14	Haunted Hill	67741	364	16.1	8.48	243.88	56.81	0.49	0.15	69.3	172	3.74	2.61	26.04	52.64	0.158	1181.1	889
30	Haunted Hill	90325	225	15.2	9.94	150.75	55.47	0.16	8.6	0	0	0.88	1	1.32	33.66	0.014	15.5	12.5
56	Haunted Hill	143749	1371	17.5	6.54	918.57	262.61	1.28	42.82	166.32	184	8.62	21.71	4.63	233.26	0.085	9	4.5
5	Latrobe Group	52754	1165	25.8	11.12	780.55	82.35	0.42	2.68	0	0	3.91		16.44	180.45	0.011	774.1	700
8	Latrobe Group	58937	658	16.4	10.61	440.86	133.98	0.44	2	55.44	66	16.96		11.47	110.72	0.1	872.4	710
13	Latrobe Group	64835	289	16.3	7.46	193.63	52.7	0.13	0.07	52.5	84	10.92		3.37	31.79	0.404	253	233
15	Latrobe Group	76074	908	16.6	7.56	608.36	229.05	0.12	0.07	54.6	128	0.62	1	9.93	120.31	0.315	825	825
16	Latrobe Group	76079	1287	16.1	10.65	862.29	368.89	1.2	0.41	23	64	44.02	5.81	61.36	208.02	0.068	730	703
17	Latrobe Group	77436	723	16.6	8.17	484.41	130.92	0.35	0.07	154.14	0	38.94	20.36	11.54	94.14	0.565	775.1	556
18	Latrobe Group	77945	1246	15.3	9.49	834.82	156.85	0.43	1.67	328.02	18	2.62	10.5	11.7	259.29	0.036	875.8	774.9
21	Latrobe Group	84155	2760	22.9	5.34	1849.2	826.15	1.94	21.25	31	0	0.58	84.22	9.7	365.09	0.513	230.1	156.4
27	Latrobe Group	89809	255	15.8	8.96	170.85	122.01	0.4	0.1	50	42	9.83	0.63	3.5	40.63	0.032	903.3	804
31	Latrobe Group	90366	1041	23.4	9.22	697.47	131.75	0.38	0.72	225	176	29.57	1.81	21.84	206.29	0.223	847.2	830
32	Latrobe Group	92118	419	14.6	8.62	280.73	93.76	0.47	0.06	47.04	130	39.85	4.32	4.61	69.69	0.113	244.3	213.6
33	Latrobe Group	96560	990	17.4	7.33	663.3	167	0.65	0.11	209.16	184	22.26	29.28	21.03	119.43	0.175	583	558
34	Latrobe Group	101217	1897	15.9	6.78	1270.99	563.6	1.91	2.13	73.5	40	19.71	52.93	5.18	270.81	0.735	38	35
35	Latrobe Group	103583	2340	25.8	6.85	1567.8	490.26	1.55	0.38	144	98	5.88	39.71	18.48	313.64	0.1	727.7	674
42	Latrobe Group	105483	324	15.2	7.36	217.08	84.11	0.33	0.02	12.18	76	20.37	2.53	3.8	33.62	0.437	1389.2	1029.1
51	Latrobe Group	110722	693	16.8	7.68	464.31	155.72	0.73	0.06	54.18	96		18.5	14.98	98.91	0.128	429	429
52	Latrobe Group	110725	427	18.3	8.59	286.09	84.95	0.35	8.88	54.18	186		2.19	6.48	59.68	0.105	740	668
53	Latrobe Group	110729	1009	17.1	7.34	676.03	216.98	0.81	6.99	139.02		63.6	28.78	5.59	112.87	0.453	114.7	114.7
54	Latrobe Group	110731	1307	16.8	6.98	875.69	251.23	1.03	8.36	235.2		70.22	62.93	5.16	122.63	0.328	199.5	199.5
10	Older Volcanics	61125	612	14.9	6.13	410.04	130.77	0.04	1.98	80.64	64	4.08	7.54	1.01	79.52	0.05	98.5	98.5
11	Older Volcanics	61160	524	17.6	7.81	351.08	63.57	0.13	1.76	145.32	170	33.61	29.61	4.92	38.63	0.197	60	55
12	Older Volcanics	61184	654	15.4	7.57	438.18	107	0.03	0.08	137.34	106	20.13	27.77	6.4	76.69	0.082	60	37.5

20	Older Volcanics	79784	612	16.6	7.13	410.04	106.4	0.35	1.79	136	122	34.76	30.44	4.03	36.92	0.149	36.6	21
46	Older Volcanics	107970	457	10.2	4.95	306.19	146.38	0	0	6.72	80	27.94	33.16	12.09	120.89	0.302	90.2	65.5
55	Older Volcanics	133352	560	17.4	7.64	375.2	73.52	0.3	1.69	145.32	170	35.7	34.24	5.48	40.19	0.231	72	58
6	Strzelecki Group	56497	683	22.9	7.5	457.61	92.35	0.28	0.48	181	108	17.48	13.07	18.08	95.19	0.991	961.2	879.1
7	Strzelecki Group	58935	325	16.8	7.87	217.75	70.12	0.21	0.08	41.58	84	15.52	4.4	3.14	38.92	0.2	862	358
50	Strzelecki Group	110720	483	14.5	6.55	323.61	126.62	0.52	0.07	11.76	76	38	5.29	4.66	46.33	0.337	333	274.9

sandstone and is considered a low hydraulic conductive aquifer; the Tambo River Formation is an aquitard of glauconite marls and marly limestones.

The Sale Group includes the Boisdale and the Haunted Hill Formations, both of which are significant aquifers. The Boisdale Formation only occurs in the basin east of Traralgon and consists of two major units; a lower Late Miocene sand unit (Wurruk Sand) and an upper Pliocene clay unit (Nuntin Clay). The sands form an aquifer in the eastern part of the basin, in particular around the town of Sale (Department of Sustainability and Environment, 2010), and can reach up to 200 m thickness with hydraulic conductivities of 24–30 m/day (Walker and Mollica, 1990; Schaeffer, 2008). The Wurruk Sands are partly confined by the Nuntin Clays in the area around Sale. The Pleistocene Haunted Hill Formation covers most of the Gippsland Basin with variable thicknesses of 5–80 m (Table 1) and is a group of interbedded alluvial gravels, sands and clays (Douglas and Ferguson, 1988). These deposits overlie the Boisdale Formation in the east and the Yallourn Formation in the west (Latrobe Valley Depression) and are a poor heterogeneous aquifer with hydraulic conductivities ranging from 0.01 to 1 m/day (Nahm, 2002).

The Quaternary deposits include recent floodplain deposits, river terraces, coastal lagoon and coastal dune deposits (Jones and Veevers, 1982). The larger rivers in the region have eroded previously deposited sediments, which form terraces up to 20 m higher than current river levels. Extensive flood plains exist in some parts of the basin, composed of alternating sand, gravel and clay deposits. Most of the sediments represent localised aquifers and are used for irrigation. Hydraulic conductivities range widely (5–300 m/day) through the Quaternary Sediments (Table 1). Coastal regions have large lagoons, consisting of poorly conductive clay-rich deposits and highly conductive sand dunes.

The Gippsland Basin is cut by major fault systems (Fig. 4). The Rosedale fault system follows the centre of the basin, while the Darriman, Wonwron and Foster fault system is located along the southern margin of the basin (Holdgate et al., 2003). Sets of anticlines and synclines occur in the Latrobe Valley and define local sub-basins. They strike SW–NE in the western part of the Valley and are E–W striking further east. The Latrobe Valley Depression is a large WSW-ENE striking syncline, which continues into the Lake Wellington Depression east of the Balook Block (Fig. 4). The Moe Swamp Basin lies west of the Latrobe Valley Depression, separated from it by the Haunted Hill Block and bound to the west by the Darnum Fault in the west (Fig. 4). The Lake Wellington Depression lies east to the Latrobe Valley Depression separated by Balook Block.

2. Sampling and analytical methods

The aquifers sampled in this study encompass the Haunted Hill Formation, Boisdale Formation, Baloock Formation, Strzelecki Group, Latrobe Group, Thorpdale Volcanics and Childers Formation. Groundwater samples are from 60 bores (Fig. 4 and Table 2) that belong to the Victorian State Observation Bore Network (Department of Sustainability and Environment, 2010) in March and May 2008. The bores have screens that are generally <6 m and sample discreet horizons in the aquifer units (Table 2). A Bennett pump was used for bores up to 100 m depth, while a bailer or impellor pump was used for some shallow or narrow cased bores. Groundwater from artesian aquifers was sampled directly at the bore heads. Depth to water was determined using an electronic water level tape. Electrical conductivity, temperature and pH, were determined in the field with Orion model 128 conductivity and model 290A pH meters and probes. Dissolved O_2 was measured using a Hach drop titration kit and is precise to ±1 mg/L. Carbonate

and bicarbonate alkalinity and dissolved CO_2 concentrations were determined by titration at the end of every sampling day using a Hach digital titrator and are precise to ±5%. Anion concentrations were determined on filtered (0.45 µm cellulose nitrate filters) unacidified samples at Monash University using a Metrohm ion chromatograph. Cation concentrations were determined on filtered samples that had been acidified with 16 M HNO_3 to pH < 2 on a Varian Vista AX CCD Simultaneous ICP-AES at the Australian National University. The precision of major ion concentrations calculated using replicate samples is ±2%. Additional major ion chemistry data for groundwater from 147 bores in a range of aquifers were taken from Victorian Water Warehouse (2011).

Stable isotope ratios were measured using Finnigan MAT 252 and DeltaPlus Advantage mass spectrometers at Monash University. The $\delta^{18}O$ was determined via equilibration with a He–CO_2 gas mixture at 32 °C for 24–48 h in a ThermoFinnigan Gas Bench by continuous flow. The δ^2H was determined by reduction with Cr at 850 °C using a Finnigan MAT H-Device. The $\delta^{18}O$ and δ^2H values were measured against internal standards, which were calibrated against International Atomic and Energy Agency (IAEA), Standard Mean Ocean Water (SMOW), Greenland Ice Sheet Precipitation (GISP) and Standard Light Arctic Precipitation (SLAP) standards. Data were normalised following Coplen (1988) and are expressed relative to V-SMOW, where $\delta^{18}O$ and δ^2H values of SLAP are −55.5‰ and −428‰, respectively. The $\delta^{13}C$ of dissolved inorganic C (DIC) was determined by acidification with H_3PO_4 in a He atmosphere in a ThermoFinnigan Gas Bench by continuous flow. The results are expressed relative to the Pee Dee Belemnite (PDB) standard. Water samples for $\delta^{34}S$ analyses were acidified to pH < 2 using 10 N distilled HNO_3 and boiled gently for ~4 h to reduce volume and remove dissolved inorganic C. An excess of $BaCl_2$ was added to the sample to precipitate $BaSO_4$, and allowed to settle overnight. The residual solution was decanted and the precipitate was rinsed with distilled water and dried. The $BaSO_4$ was combusted to SO_2 with V_2O_5 in a Carlo Erba 1110 Flash EA and $\delta^{34}S$ values were measured by continuous flow. Standardisation of $\delta^{34}S$ to the Cañon Diablo Troilite (CDT) scale was via analysis of NBS-127 and IAEA-SO5. Precision (1σ) based on replicate analyses is 0.15‰ for $\delta^{18}O$, 1‰ for δ^2H, 0.2‰ for $\delta^{13}C$, and 0.2‰ for $\delta^{34}S$.

The $^{87}Sr/^{86}Sr$ ratios of groundwater were measured at the University of Adelaide. Sufficient water to yield a minimum of 1–2 µg Sr was evaporated to dryness. The residue was dissolved in 2 mL of 6 M HCl, evaporated to dryness, and re-dissolved in 2 M HCl. Strontium was extracted from centrifuged supernatant using cation exchange columns and Biorad AG50W X8200-400 mesh resin. Isotope analysis was carried out on a Finnigan MAT 262 thermal spectrometer in static mode. Samples for ^{14}C and ^3H were analysed at the Institute for Environmental Research of the Australian Institute of Nuclear Science and Engineering (AINSE) facilities at Lucas Heights, Sydney, Australia, using Accelerator Mass Spectrometry (AMS) for ^{14}C after acid extraction and graphitisation of inorganic C and liquid scintillation spectrometry (Perkin Elmer 1220 Quantulus) for ^3H after pre-concentration through electrolysis The ^3H analysis is described in detail in Neklapilova (2008a,b). The concentrations for ^{14}C are expressed as percent modern C (pMC) and the 1σ precision of $^{14}C/^{12}C$ ratios is ±0.05%. Ages were calculated using after the method of Stuiver and Polach (1977).

3. Results and discussion

3.1. Groundwater flow

The general groundwater flow direction follows topography from the basin margins eastwards along the axis of the basin and from the outer mountain margins of the basin towards the centre (Fig. 3a and b). The impact on flow from dewatering of the coal pits in the centre of the basin is apparent with the development of a groundwater depression and consequent modification of groundwater flow paths. While coal mining began in the 1920s, intensive groundwater monitoring did not commence until the 1980s. Groundwater levels in the Latrobe Group have fallen by approximately 20 m in bores around the coal pits between 1980 and 2010. A comparison between head data from 1990 and 2008 in the Latrobe Group indicates that the cone of depression was located around Morwell in the 1990s and spread to the west towards Traralgon, where head values dropped by 68 m between 1990 and 2008 (Fig. 3a). Local groundwater flow direction changed in the area around Morwell and Traralgon with flow directions shifting toward the cone of depression. Furthermore, the water divide around the Balock Block shifted to the west as a consequence of the decreasing water levels in the area around the coal mines.

Groundwater levels in the Boisdale formation further east towards Sale declined by 5–10 m between 1990 and 2008. Most data for the Boisdale Formation is available for the area around Sale and Lake Wellington. The general groundwater flow direction still follows the topography towards the coast, despite the decline in water levels (Fig. 3b). The low groundwater levels around Lake Wellington suggest that groundwater from the Boisdale Formation drains into the lake.

Away from the groundwater depression, the overall hydraulic gradient in the western part of the Latrobe Valley is ~1.25×10^{-3}, while that in the Lake Wellington area in the eastern part of the basin is lower (~3×10^{-4}). Vertical hydraulic gradients are typically downward in the west of the Latrobe Valley, ranging from 1.4×10^{-5} to 2.5×10^{-8}. Vertical head gradients in the western end of the Latrobe Valley are downward, implying downward flow. By contrast head gradients are upward in the east suggesting upward flow from deeper to shallower units. The upward head gradients are locally large especially in the area around the Gippsland Lakes where some groundwater is artesian.

3.2. Major ion chemistry

Groundwater in all aquifers in the Latrobe Valley has generally low salinity, with total dissolved solids (TDSs) < 4500 mg/L and is of Na–K–Ca–HCO_3–Cl type. Generally lower salinity groundwater <500 mg/L occurs in the western part of the basin, whereas groundwater closer to Lake Wellington in the East and to the coast mostly has the higher salinities (>1000 mg/L) and changes to a Na–Cl type. The higher TDS contents and predominance of Na–Cl type groundwater in the shallow units near the coast may be caused by saltwater intrusion. Groundwater from the shallow aquifers generally has TDS contents >2000 mg/L. While groundwater has a wide range of TDS, there is little correlation of TDS with distance from the basin margins ($r^2 = 0.13$). The pH of the groundwater has a range of 4.9–11.2. Shallow groundwater generally contains dissolved O_2 (DO), while deeper groundwater is generally anoxic. Sodium is generally the most abundant cation representing between 40% and 99% of relative molar cation concentrations. Chloride concentrations vary between 30% and 98%. The proportion of Na and Cl relative to other ions increases with increasing TDS. Despite the variable aquifer lithologies, which include limestones, clastic sediments and coal seams, the major ion chemistry of groundwater in all aquifers is similar across the basin and there are no systematic changes along the flow paths (Fig. 5).

Major ion geochemistry may be used to determine the predominant hydrogeochemical processes. Because the geochemistry of the groundwater in the Latrobe Valley is similar between the different aquifers and does not vary significantly with position in the basin, the geochemistry will be discussed for the groundwater as a whole.

Molar Cl/Br ratios in the groundwater in the Latrobe Valley range from 24 to 1574 (Fig. 6a). Aside from groundwater in the Thorpdale Volcanics that has lower Cl/Br ratios (24–786), Cl/Br ratios in groundwater from the different aquifers are similar (Fig. 6a). The Cl/Br ratios of coastal rainfall are generally 600–650, similar to those of ocean water (Davis et al., 1998). A range of processes can modify the Cl/Br ratios of precipitation. The Cl/Br ratios of inland rain may be lower due to the removal of marine aerosols in early precipitation (Davis et al., 1998). Bromine is also bound to humus in soils and the decomposition of organic matter may release Br, so reducing Cl/Br ratios significantly (Gerritse and George, 1988). By contrast halite dissolution results in Cl/Br ratios of ~10,000 (Herczeg and Edmunds, 2000; Cartwright et al., 2006). The observation that the Cl/Br ratios do not increase with increasing Cl concentrations indicates that no significant halite dissolution has occurred

(c.f., Davis et al., 1998; Herczeg and Edmunds, 2000; Cartwright et al., 2004; Alcala and Custodio, 2008). The scatter of Cl/Br ratios around those of rainfall indicates that there may be minor halite dissolution and/or cycling of Br through organic matter. Molar Na/Cl ratios are up to 7 in the lowest salinity groundwater of some parts of the Thorpdale Volcanics and parts of the Childers Formation (TDS < 1000 mg/L) but close to those of seawater (0.86) and local rainfall (0.5–1.0) in more saline groundwater, for example in the Boisdale Formation (Fig. 6b). Other cations (such as K, Ca, and Mg) have similar trends (Fig. 7c and d).

Calcium and Mg concentrations from the Thorpdale Volcanics and the Childers Formation are strongly correlated ($r^2 = 0.86$) in comparison to the other units. With a moderate correlation between Ca and HCO_3 and Ca and SO_4, the source of Ca and Mg is likely to be mainly from weathering of high MgO and CaO silicate
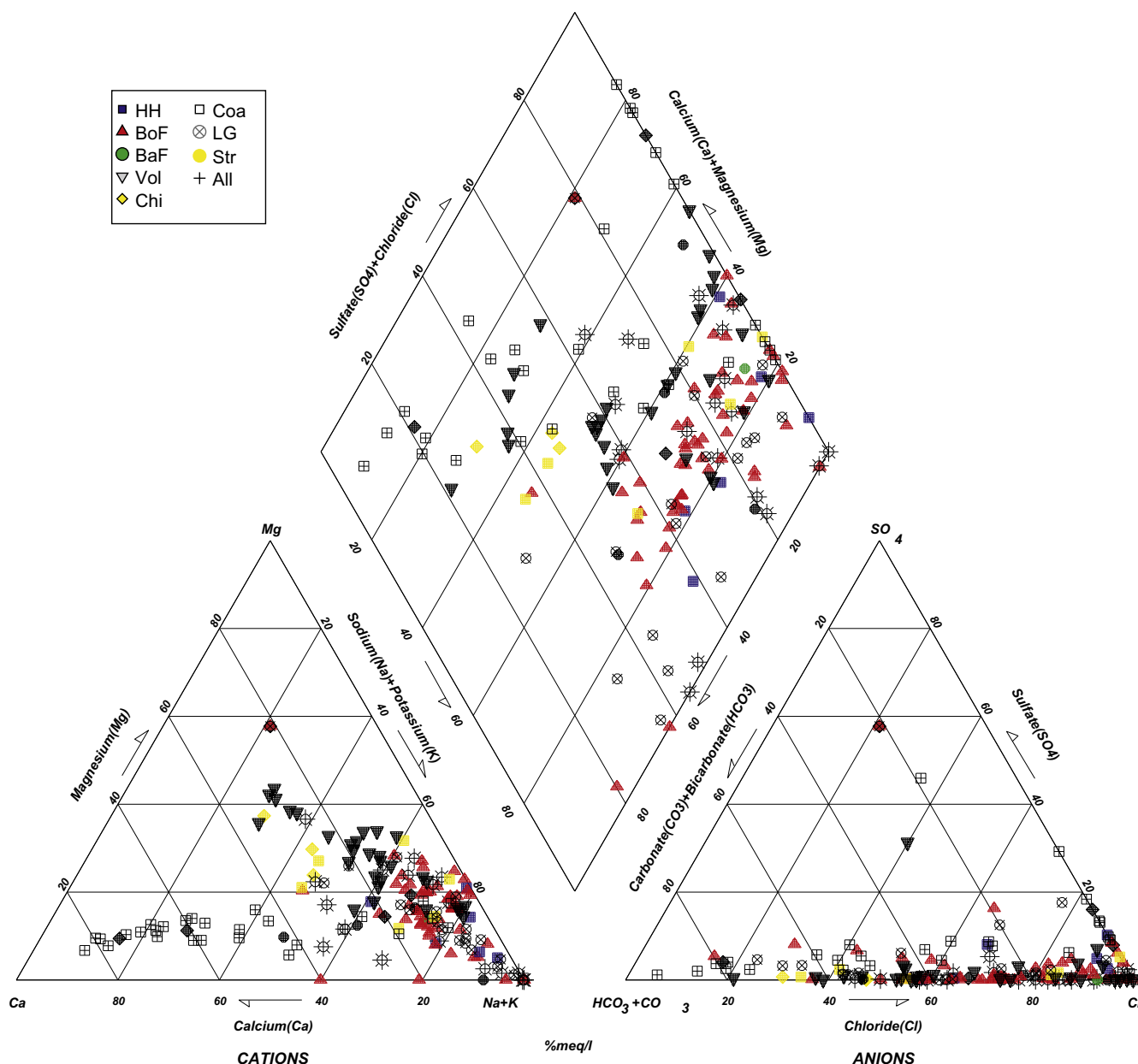
Fig. 5. Piper diagram showing proportions of major ions in groundwater from the Gippsland Basin. The majority of groundwater in the aquifers is Na and Cl dominated. The plotted data incorporates the sample bores in this study and additional groundwater data from the Victorian Water Warehouse (2011). (Abbreviations: HH – Haunted Hill Formation, BoF – Boisdale Formation, BaF – Ballok Formation, Vol – Thorpdale Volcanics, Chi – Childers Formation, Coa – Coastal Dunes, LG – Latrobe Group, Str – Strzelecki Formation, All – Alluvial deposits).

minerals, for example plagioclase and mafic minerals in the basalts. The Thorpdale Volcanics consist mostly of olivine basalt (Douglas and Ferguson, 1988), while the Childers Formation is composed of terrestrial alluvial deposits. The sediments of the Childers Formation interfinger with the Thorpdale Volcanics and both are likely to be hydraulically connected. Calcium is correlated with
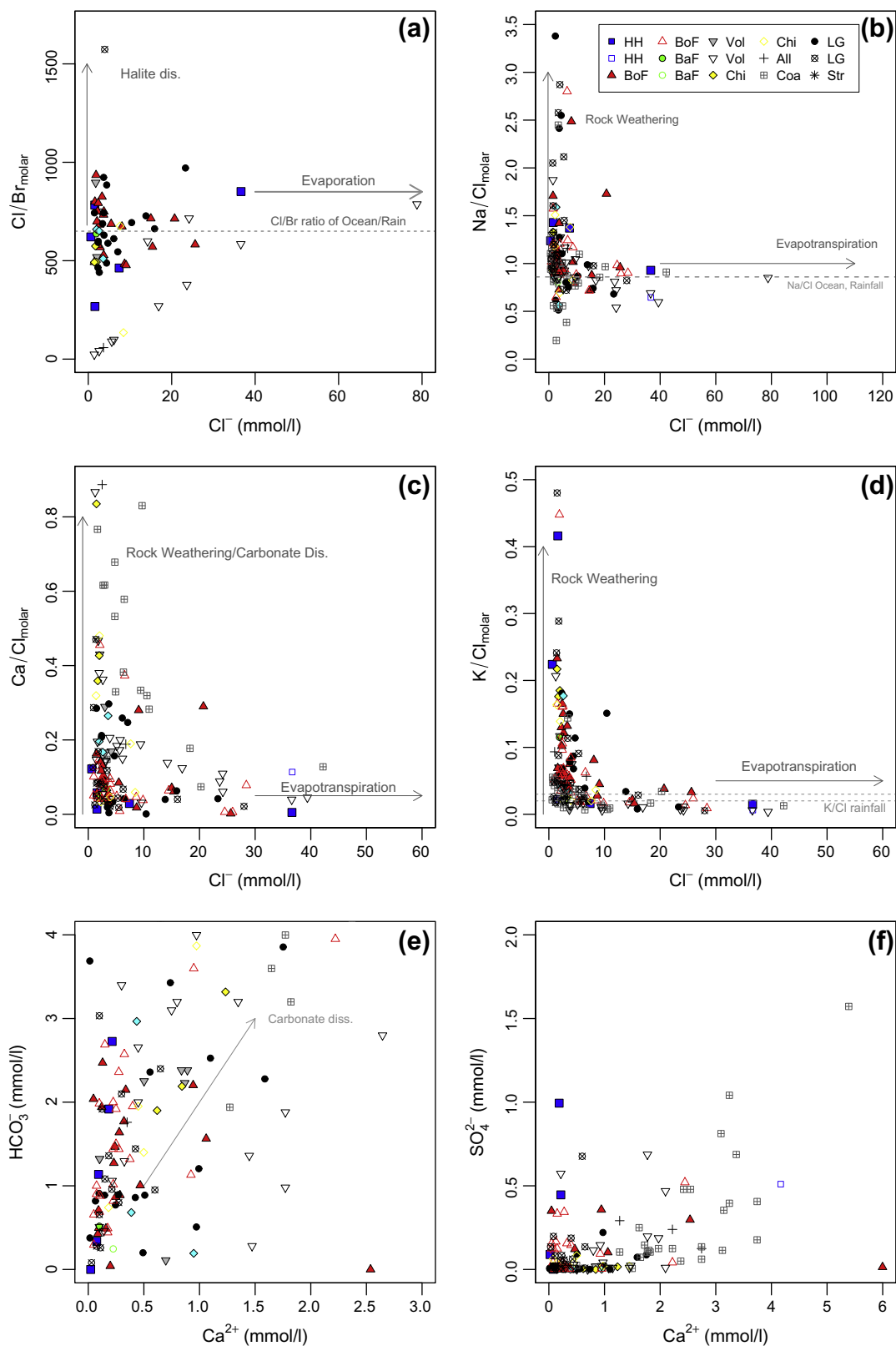
Fig. 6. (a) Molar Cl/Br, (b) molar Na/Cl, molar Ca/Cl and molar K/Cl ratios versus Cl indicating the importance of evaporation and rock weathering on the groundwater from the Gippsland Basin. (e) HCO_3^- and SO_4^{2-} versus Ca showing that calcite dissolution is a minor process. (Abbreviations: HH – Haunted Hill Formation, BoF – Boisdale Formation, BaF – Ballok Formation, Vol – Thorpdale Volcanics, Chi – Childers Formation, Coa – Coastal Dunes, LG – Latrobe Group, Str – Strzelecki Formation, All – Alluvial deposits).

Na and K, supporting the conclusion that the source of the cations is mainly from silicate weathering. A possible source for Na and K in the Latrobe Group, Boisdale Formation and Haunted Hill Formation is the weathering of feldspar (Alkali feldspar) in sediments that derive from the Palaeozoic basement and the granite intrusions in the Alpine Region.

The geochemistry data imply that mineral weathering influences the geochemistry of the lower salinity groundwater but that evapotranspiration is the dominant process in groundwater with higher TDS. It is most likely that only low levels of evapotranspiration occur during direct recharge on the basin margins, while the high saline groundwater in the younger units suggests that evapotranspiration of shallow groundwater is significant. Calcium and HCO_3 are weakly correlated ($r^2 = 0.01$) and do not follow a 1:2 trend, indicating that calcite dissolution does not control the geochemistry of the groundwater (Herczeg and Edmunds, 2000) (Fig. 6e). Bicarbonate, which is the more dominant anion in groundwater with TDS < 500 mg/L, is most likely derived from dissolution of soil CO_2. Similarly the lack of correlation between Ca and SO_4 ($r^2 = 0.38$) implies that that gypsum dissolution is not a dominant geochemical process (Fig. 6f). Most groundwater is under saturated with respect to calcite (SI from -4.33 to 0) and dolomite (-8.45 to 0). Ten groundwater samples, mainly from the Boisdale Formation and Latrobe Group, are saturated with respect to calcite (SI from 0 to 1.29) and dolomite (SI from 0 to 1.97).

The groundwater from the Haunted Hill Formation has the highest average Na and Cl concentrations (1031 mg/L Na; 1298 mg/L Cl) and low Na/Cl ratios (0.92–1.37), indicating that the shallow groundwater is strongly influenced by evapotranspiration. Silicate weathering, calcite, and gypsum dissolution appear to be minor processes that influence mainly the geochemistry of the lower salinity groundwater. Despite very different lithologies groundwater from the different aquifers in the Latrobe Valley has very similar major ion geochemistry without a distinct spatial pattern. The lack of chemical differentiation between groundwater suggests that most aquifers are connected and that inter-aquifer mixing occurs.

3.3. Stable isotopes

3.3.1. $\delta^{18}O$ and δ^2H

Groundwater $\delta^{18}O$ values range from $-6.7‰$ to $-2.5‰$ and δ^2H values range from $-44‰$ to $-20‰$, respectively (Table 3). The $\delta^{18}O$ and δ^2H values are similar across the aquifers (Fig. 7). While most groundwater has $\delta^{18}O$ and δ^2H values that are close to the meteoric water line, some samples from the Boisdale Formation, the Latrobe Group and the Haunted Hill Formation lie to the right of the MWL (Fig. 7). The displacement of $\delta^{18}O$ and δ^2H values to the right of the meteoric water line probably reflects evaporation, which was inferred as the major geochemical process from the major ion geochemistry.

3.3.2. $\delta^{13}C$ and $^{87}Sr/^{86}Sr$

Carbon and Sr isotopes are commonly used in conjunction with each other to constrain carbonate dissolution, inter-aquifer mixing, and water–rock interaction. The $^{87}Sr/^{86}Sr$ ratios in groundwater vary with aquifer mineralogy. Strontium-87 is produced by the decay of ^{87}Rb, and $^{87}Sr/^{86}Sr$ ratios are controlled by the initial $^{87}Sr/^{86}Sr$ and the $^{87}Rb/^{87}Sr$ ratio of the minerals and their ages (McNutt, 2000). As Rb substitutes for K and Sr substitutes for Ca, minerals rich in Ca such as calcite generally have low $^{87}Sr/^{86}Sr$ ratios (Katz and Bullen, 1996) while K-bearing minerals such as K-feldspar have higher $^{87}Sr/^{86}Sr$ ratios. Other silicates (such as plagioclase) have intermediate $^{87}Sr/^{86}Sr$ ratios. The $^{87}Sr/^{86}Sr$ ratios of young basaltic igneous rocks are generally similar to that of the Earth's mantle $\sim$0.701 (Clark and Fritz, 1997; Quade et al., 1995).
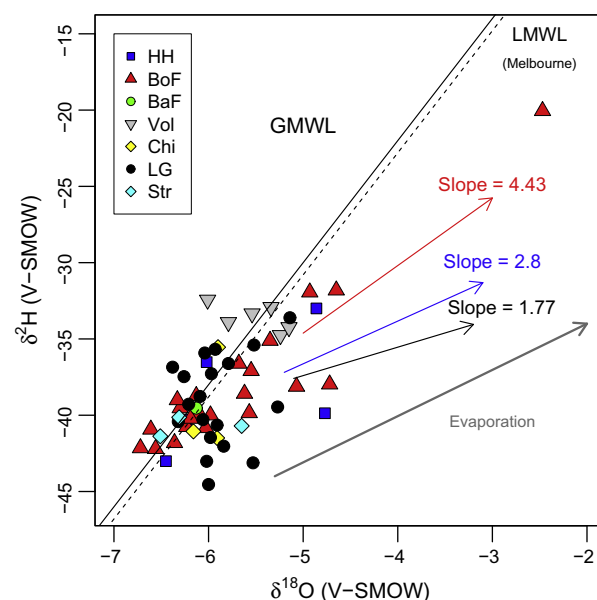
Fig. 7. δ^2H versus $\delta^{18}O$ for the sampled groundwater in the Gippsland Basin. The arrows indicate the slope of the trend line for samples from specific aquifer units. (Abbreviations: HH – Haunted Hill Formation, BoF – Boisdale Formation, BaF – Ballok Formation, Vol – Thorpdale Volcanics, Chi – Childers Formation, LG – Latrobe Group, Str – Strzelecki Formation).

The $^{87}Sr/^{86}Sr$ of seawater has fluctuated between $\sim$0.7070 and $\sim$0.7092 and marine calcite has $^{87}Sr/^{86}Sr$ ratios closely similar to that of the oceans when it was formed. Modern seawater has e$^{87}Sr/^{86}Sr$ ratios of $\sim$0.709 (Clark and Fritz, 1997). Potassium-bearing silicates have $^{87}Sr/^{86}Sr$ ratios dependant on their Rb/Sr ratio and age and are commonly >0.740 (McNutt, 2000). Thus, groundwater that has dissolved predominantly silicates is expected to have high $^{87}Sr/^{86}Sr$ ratios and low $\delta^{13}C$ values due to C being derived from soil CO_2. By contrast, groundwater that has dissolved carbonate minerals is expected to have low $^{87}Sr/^{86}Sr$ ratios and relatively high $\delta^{13}C$ values (Faure and Mensing, 2004; Katz and Bullen et al., 1996; Dogramaci and Herczeg, 2002; Cartwright et al., 2007a). In many aquifer systems, the dissolution of varying proportions of silicates and carbonates results in $^{87}Sr/^{86}Sr$ ratios and $\delta^{13}C$ values defining coherent trends between these two end members.

The Sr concentrations in groundwater from the Latrobe Valley range from 0.01 to 1.9 mg/L and are moderately correlated with Ca concentrations ($r^2 = 0.51$). The $^{87}Sr/^{86}Sr$ ratios vary from 0.7048 to 0.7186 (Table 3). Groundwater from the Boisdale Formation and the Latrobe Group has the largest range of $^{87}Sr/^{86}Sr$ ratios (0.707–0.719). In comparison, $^{87}Sr/^{86}Sr$ ratios in groundwater from the Thorpdale Volcanics and the Childers Formation are <0.712, with most <0.709. The low $^{87}Sr/^{86}Sr$ ratios in the groundwater from the Thorpdale Volcanics most probably reflect weathering of minerals in the basalt, while low $^{87}Sr/^{86}Sr$ ratios in the Latrobe Group probably reflect weathering of the limestone. Higher $^{87}Sr/^{86}Sr$ ratio groundwaters from the Boisdale Formation and the Latrobe Group probably indicate silicate weathering. However, as with the major ion geochemistry there is considerable overlap between the $^{87}Sr/^{86}Sr$ ratios of groundwater from different aquifers.

The $\delta^{13}C$ values of DIC reflect evolution occurring during recharge and subsequent geochemical processes in the aquifers. The $\delta^{13}C$ values in recharge typically are controlled by the dissolution of CO_2 from the soil zone. Organic C in soils in SE Australia is largely derived from C3 vegetation and has $\delta^{13}C$ values of $-30‰$ to $-25‰$ (Quade et al., 1995). There is a $\sim$4‰ enrichment in $\delta^{13}C$ values of soil CO_2 over those of the organic matter from which it is derived (Cerling et al., 1989; Emblanch et al., 2003), thus the $\delta^{13}C$

Table 3
Stable isotope data table for the sampled groundwater in the Latrobe Valley.

No.	Formation	Site name	$\delta^{18}O$ ‰ SMOW	$\delta^{2}H$ ‰ SMOW	$\delta^{13}C$ ‰ PDB	$^{87}Sr/^{86}Sr$	$\delta^{34}S$ ‰ CTD
40	Balook Formation	105134	−6.13	−39.53	26.64	0.71018	
3	Boisdale Formation	50876	−6.03	−40.83	−13.21	0.70947	41.69
4	Boisdale Formation	52753	−6.3	−39.53	−2.39	0.71517	
9	Boisdale Formation	59308	−5.68	−36.61	−14.81		22.26
19	Boisdale Formation	77947	−5.55	−37.09	−15.98		
22	Boisdale Formation	86464	−6.72	−42.15	−15.33		
23	Boisdale Formation	86465	−5.57	−39.85	−18.43		15.63
24	Boisdale Formation	86466	−5.62	−38.58	−16.92		
25	Boisdale Formation	86669	−6.36	−41.81	3.84		
26	Boisdale Formation	86670	−6.61	−40.93	−7.24	0.7165	
28	Boisdale Formation	90148	−6.23	−40.76	−10.86		
29	Boisdale Formation	90149	−6.33	−39	−5.81	0.71244	
36	Boisdale Formation	103811	−4.93	−31.94	−15.9		12.75
37	Boisdale Formation	103820	−2.47	−20.05	−20.05		12.66
38	Boisdale Formation	103822	−6.13	−38.73	4.57		23.11
39	Boisdale Formation	105132	−6.1	−39.88	6.3	0.71684	
41	Boisdale Formation	105196	−6.56	−42.2	2.07		8.11
43	Boisdale Formation	105484	−4.65	−31.81	−16.78	0.7089	
44	Boisdale Formation	105547	−6.19	−40.22	−12.91		
45	Boisdale Formation	105548	−5.98	−40	4.21	0.71216	
57	Boisdale Formation	145091	−4.72	−37.97	−22.97	0.71861	13.16
58	Boisdale Formation	145092	−5.07	−38.12	−12.94	0.70982	
59	Boisdale Formation	145093	−5.35	−35.11	−0.6		21.52
47	Childers Formation	107971	−5.9	−35.54	−17.7	0.70801	
48	Childers Formation	107972	−6.16	−41.06	−12.74	0.7066	
49	Childers Formation	107973	−5.91	−41.49	−20.56	0.71195	
1	Haunted Hill	23726	−6.02	−36.52	−31.1		
2	Haunted Hill	45759	−4.86	−33	−11.79		20.43
14	Haunted Hill	67741	−6.45	−43.01	−2.8		14.25
30	Haunted Hill	90325	−6.23	−40.29	−16.28	0.71041	26.65
56	Haunted Hill	143749	−4.77	−39.87	−13.42		26.5
5	Latrobe Group	52754	−6.38	−36.85	−6.18	0.70859	38.83
8	Latrobe Group	58937	−5.91	−40.65	−12.38	0.71397	13.92
13	Latrobe Group	64835	−6.04	−35.92	−0.75	0.70932	
15	Latrobe Group	76074	−6.21	−39.28	11.68		
16	Latrobe Group	76079	−5.93	−35.68	−17	0.71161	21.71
17	Latrobe Group	77436	−5.97	−37.28	−18.91	0.70819	
18	Latrobe Group	77945	−6.02	−43.02	1.98		32.16
21	Latrobe Group	84155	−5.52	−35.4	−12.14		16.06
27	Latrobe Group	89809	−6.32	−40.42	−6.31	0.71323	20.41
31	Latrobe Group	90366	−6.06	−40.29	−7.3	0.7084	18.53
32	Latrobe Group	92118	−6.09	−38.77	13.38	0.70887	21.73
33	Latrobe Group	96560	−5.79	−36.61	−14.57	0.71459	17.56
34	Latrobe Group	101217	−5.14	−33.61	−14.88		24.39
35	Latrobe Group	103583	−5.98	−41.46	0.63	0.71327	
42	Latrobe Group	105483	−6.26	−37.47	−5.8		
51	Latrobe Group	110722	−5.53	−43.12	0.37		
52	Latrobe Group	110725	−6	−44.54	−11.17		
53	Latrobe Group	110729	−5.84	−42.03	−20.27	0.71025	25.38
54	Latrobe Group	110731	−5.27	−39.46	−16.97	0.70772	38.71
10	Older Volcanics	61125	−6.01	−32.44	−18.43	0.708	30.2
11	Older Volcanics	61160	−5.15	−34.24	−22.74		25.25
12	Older Volcanics	61184	−5.54	−33.34	−15.41	0.70482	
20	Older Volcanics	79784	−5.34	−32.92	−18.21	0.70491	23.08
46	Older Volcanics	107970	−5.79	−33.91	−15.23		43.51
55	Older Volcanics	133352	−5.24	−34.76	−20.56		17.65
6	Strzelecki Group	56497	−6.51	−41.38	−13.04		
7	Strzelecki Group	58935	−6.31	−40.14	−2.29	0.71192	
50	Strzelecki Group	110720	−5.65	−40.7	−15.72		48.57

values of soil CO_2 is predicted to be −26‰ to −21‰. At 20 °C and pH 7, $\delta^{13}C$ values of DIC calculated from the fractionation data of and Mook et al. (1974) is −20‰ to −16‰. The $\delta^{13}C$ values of DIC in groundwater in the Gippsland Basin range from −31.1‰ to +26.7‰ (Table 3), although most range from −16‰ to −10‰ (Fig. 8b and c). The wide range of $\delta^{13}C$ values implies that there has been considerable modification of DIC post recharge. The highest $\delta^{13}C$ variations occur in the Boisdale Formation and the Latrobe Group with values ranging from −22.9‰ to +6.3‰ (mean = −9.2, median = −12.9‰) and −20.3‰ to +13.4‰ (mean = −7.2, median = −7.3‰), respectively. The sample from the Balook Formation

has the highest $\delta^{13}C$ value with +26.6‰. Generally, there is no correlation with major ion chemistry; however, the lower $\delta^{13}C$ values occur in groundwater with higher HCO_3 concentrations, especially in the Childers Formation and the Thorpdale Volcanics (Fig. 8c). Groundwater with $\delta^{13}C$ values < −10‰ occurs mainly in the Thorpdale Volcanics, the Strzelecki Group, the Childers Formation, the Haunted Hill Formation, the Boisdale Formation and the Latrobe Group.

The lack of correlation between $^{87}Sr/^{86}Sr$ ratios and $\delta^{13}C$ values together with the locally high $\delta^{13}C$ values implies that the variation of these isotopes cannot be explained simply by the groundwater
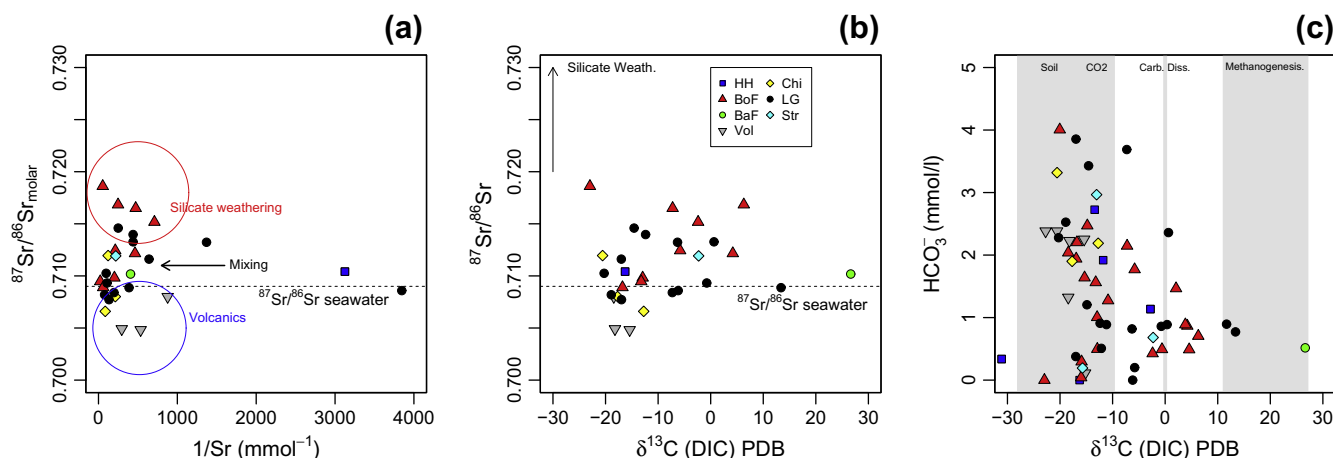
Fig. 8. (a) $^{87}Sr/^{86}Sr$ versus $1/Sr$ and (b) $^{87}Sr/^{86}Sr$ versus $\delta^{13}C$. (c) HCO_3^- versus $\delta^{13}C$ indicating that most samples have soil $\delta^{13}C$ values and some have changed due to methanogenesis and SO_4 reduction. (Abbreviations: HH – Haunted Hill Formation, BoF – Boisdale Formation, BaF – Ballok Formation, Vol – Thorpdale Volcanics, Chi – Childers Formation, LG – Latrobe Group, Str – Strzelecki Formation).

dissolving varying proportions of silicate and carbonate minerals. Methanogenesis impacts $\delta^{13}C$ values but not $^{87}Sr/^{86}Sr$ ratios and thus may cause decoupling of $^{87}Sr/^{86}Sr$ ratios and $\delta^{13}C$ values (Fig. 9a and b). There are two main biogenic methanogenesis processes. Firstly, the breakdown of long chain organic molecules that leads eventually to acetate fermentation and which has a net reaction of the form:

$$2CH_2O \rightarrow CO_2 + CH_4 \qquad (1)$$

Secondly, the direct reduction of dissolved CO_2 in the groundwater via:

$$CO_2 + 4H^+ \rightarrow CH_4 + 2H_2O \qquad (2)$$

(Clark and Fritz, 1997; Valentine et al., 2004; Leybourne et al., 2006). Carbon-13 fractionations between CO_2 and CH_4 are up to 80‰. During acetate fermentation, $\delta^{13}C$ values of DIC increase due to the dissolution of CO_2 generated by reaction (Eq. (1)), while reduction of dissolved CO_2 causes an increase in the $\delta^{13}C$ values of the residual CO_2. The high $\delta^{13}C$ values occur in the aquifers of the Latrobe Group and the Boisdale Formation that contain large coal deposits and methanogenesis commonly occurs in low-maturity

coal seams (Strapoc et al., 2011). Thus, the locally high $\delta^{13}C$ values in the groundwater from the Latrobe Valley are most probably due to methanogenesis.

If methanogenesis has occurred, bacteriological reduction of other oxidised species such as SO_4 is also likely. Much of the groundwater, especially that with high $\delta^{13}C$ values has very low SO_4 concentrations and S/Cl ratios, and $\delta^{34}S$ values as high as 48.6‰ (Fig. 9). Rainfall in SE Australia has $\delta^{34}S$ values of 15–23‰ (Dogramaci and Herczeg, 2002) and enrichment of $\delta^{34}S$ values above this is consistent with bacterial SO_4 reduction (Fig. 9b). DIC with very low $\delta^{13}C$ values may also be produced from organic matter during SO_4 reduction (Leybourne et al., 2006) via:

$$2CH_2O + SO_4 = H_2S + 2HCO_3 \qquad (3)$$
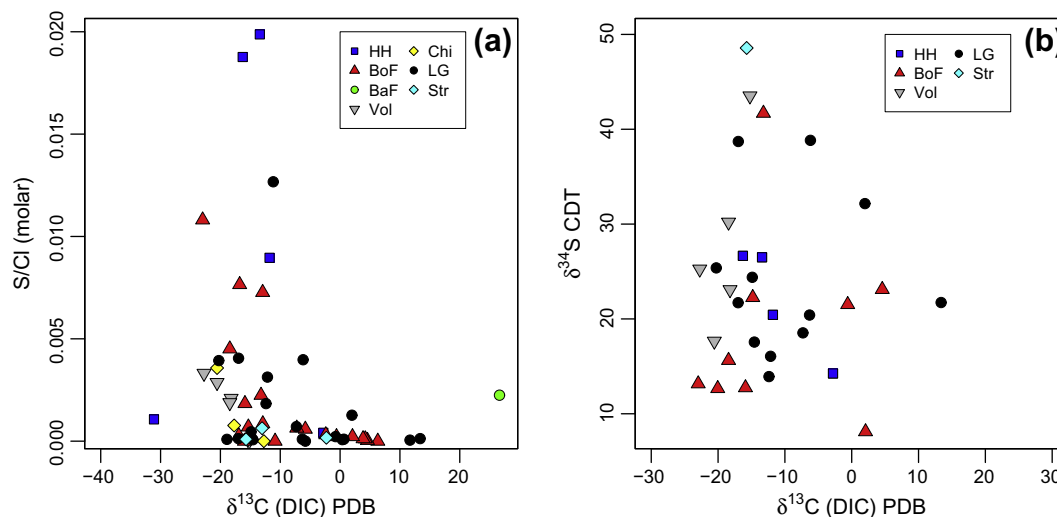
The locally low S/Cl ratios and $\delta^{13}C$ values from the Haunted Hills and Boisdale Formations may reflect this process (Fig. 10a).

3.4. Radiogenic isotopes

3.4.1. Tritium
Tritium activities in all samples are lower than those of modern rainfall, which was estimated at ~4 TU for Melbourne by Cartwright et al. (2007b) and Adelaide by Cook et al. (1994) and most

Fig. 9. (a) S/Cl ratio versus $\delta^{13}C$ and $\delta^{34}S$ versus $\delta^{13}C$ indicating that SO_4 reduction is reasonable for samples with high $\delta^{13}C$ values. (Abbreviations: HH – Haunted Hill Formation, BoF – Boisdale Formation, BaF – Ballok Formation, Vol – Thorpdale Volcanics, Chi – Childers Formation, LG – Latrobe Group, Str – Strzelecki Formation).
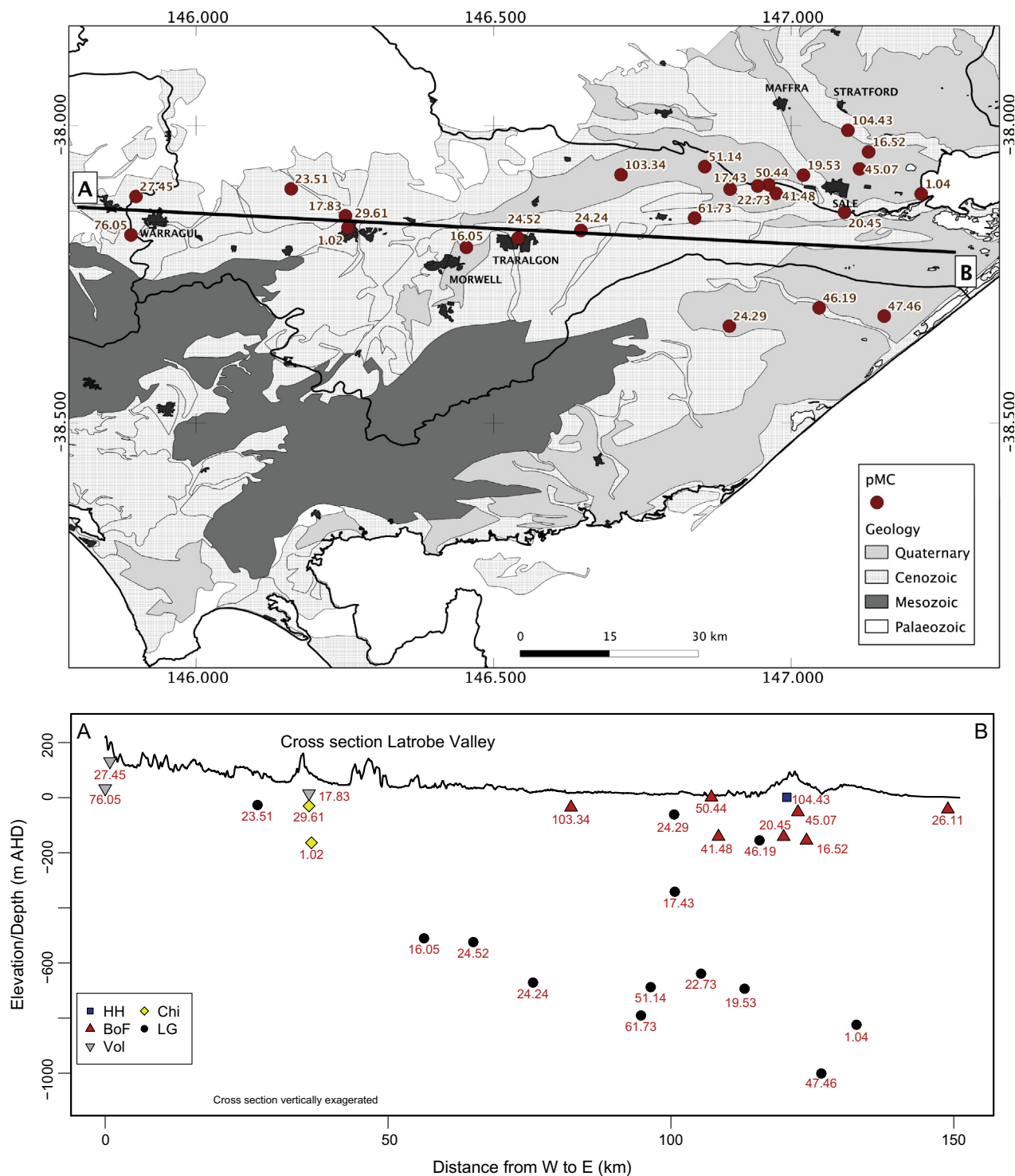
Fig. 10. Map and cross section showing the distribution of pMC across the Latrobe Valley and with depth (Table 4). (Abbreviations: HH – Haunted Hill Formation, BoF – Boisdale Formation, Vol – Thorpdale Volcanics, Chi – Childers Formation, LG – Latrobe Group).

of them are below detection (0.1 TU) (Table 4). Only two groundwater samples have ^{3}H activities greater than 0.1 TU. Groundwater in Bore 103811 (Boisdale Formation) and Bore 143749 (Haunted Hill Formation) has values of 0.6 and 1.5 TU, respectively (Table 3). This groundwater likely contains a component of water recharged during or following the atmospheric nuclear tests in the 1950s and 1960s, while groundwater with activities under 0.1 TU was recharged prior to this time.

3.4.2. Radiocarbon

The a^{14}C of DIC in the aquifers vary between 1.02 and 104.40 pMC (Table 5). The a^{14}C in the Boisdale Formation range from 16.5 to 103.3 pMC, while a^{14}C in the Latrobe Group range from 10.4 to 61.7 pMC. Groundwater from the Childers Formation has lower a^{14}C (29.61 pMC), while groundwater from the Thorpdale Volcanics has a^{14}C of 17.8–76.1 pMC. The highest a^{14}C of 103.3 and 104.4 pMC, respectively, occur in groundwater from

Table 4
³H results for selected bores in the Latrobe Valley.

Bore ID	Sample No.	Tritium Act. (TU)	Uncertainty (TU)	Quantification Limit (TU)
50876	1	0.1	0.1	0.6
61125	2	0.1	0.1	0.6
61160	3	0.1	0.1	0.7
61184	4	0.1	0.1	0.6
67741	5	0.1	0.1	0.6
86670	6	0.1	0.1	0.6
90325	7	0.1	0.1	0.6
101217	8	0.1	0.1	0.6
103811	9	0.6	0.1	0.6
105132	10	0.1	0.1	0.6
133352	11	0.1	0.1	0.6
143749	12	1.5	0.1	0.6

the shallow Haunted Hill Formation and the Boisdale Formation, in groundwater that contains measurable ³H (Table 4). The a¹⁴C do not decrease systematically within aquifers along the flow path through the basin and with depth, implying that flow systems may be complex (Fig. 10).

As noted above, ¹⁴C dating is not without problems, for example nuclear bomb testing in the 1960s increased a¹⁴C and resulted in elevated a¹⁴C in groundwater recharged during that time. More importantly for deeper groundwater, carbonate dissolution, methanogenesis via acetate fermentation, and SO_4 reduction involving organic matter, reduces a¹⁴C (Plummer and Sprinkle, 2001; Aravena et al., 1995; Aravena and Robertson, 1998; Clark and Fritz, 1997; Van der Kemp, 2000; Coetsiers and Walraevens, 2009; Cartwright et al., 2010; Hoque and Burgess, 2012). Failure to account for these processes may lead to incorrect ¹⁴C ages. The major ion and stable isotope geochemistry suggest that carbonate dissolution, SO_4 reduction and methanogenesis have occurred in some parts of the aquifer system in the Latrobe Valley; the potential impact of each process will be assessed separately.

Given that $\delta^{13}C$ values are impacted by several processes; it is difficult to apply simple mass balance calculations based on $\delta^{13}C$

values to correct for calcite dissolution. The major ion geochemistry and the lack of coherent trends in ⁸⁷Sr/⁸⁶Sr ratios versus $\delta^{13}C$ values imply that calcite dissolution does not control the geochemistry of the groundwater. Additionally, all groundwater is undersaturated with respect to calcite implying that calcite precipitation has not occurred. Approximately a third of the samples have Ca/Cl ratios equal to or slightly lower than those in rainfall (Fig. 6) (Backburn and McLeod, 1983; Ayers and Ivey, 1988) again implying that the majority of the Ca is derived from rainfall rather than calcite dissolution. In common with most studies of ¹⁴C dating in groundwater from siliclastic aquifers (Fritz et al., 1991; Cartwright et al., 2007b), it is considered that calcite dissolution accounts for no more than 15% of the DIC in this system.

Methanogenesis may have taken place via the reduction of DIC and/or acetate fermentation and as discussed above both processes increase $\delta^{13}C$ values. Because of the large ¹³C fractionations between DIC and CH_4, the production of a small amount of CH_4 during DIC reduction will significantly increase the $\delta^{13}C$ value of the residual DIC. The mass-dependant fractionation of ¹⁴C relative to ¹²C is ~2.3 times that of ¹³C (Saliege and Fontes, 1984). Thus, an increase in $\delta^{13}C$ of 15‰ should result in an increase in a¹⁴C of ~3.5%, which has only a minor impact on ¹⁴C ages. Acetate fermentation, however, introduces CO_2 derived from old organic matter from the aquifer matrix into the groundwater, which will reduce a¹⁴C. A maximum dilution factor was calculated assuming that acetate fermentation was the sole process increasing $\delta^{13}C$ values using:

$$q_{CH4} \frac{\delta^{13}C_{DIC} - \delta^{13}C_{DIC-CH4}}{\delta^{13}C_r - \delta^{13}C_{DIC-CH4}} \tag{4}$$

where q is the proportion of C derived from the atmosphere or the soil zone, $\delta^{13}C_{DIC-CH4}$ is the $\delta^{13}C$ of DIC produced by methanogenesis and $\delta^{13}C_r$ is the $\delta^{13}C$ of recharge. Coal in the Latrobe Valley has $\delta^{13}C$ values of −24‰ to −26‰ (Holdgate et al., 2009) and using the fractionation factor between CO_2 and CH_4 of 1.077 (77‰) (Whiticar et al., 1986; Koschorreck et al., 2008) implies $\delta^{13}C_{DIC-CH4}$ of ~ +14‰.

Table 5
Carbon age correction for ¹⁴C with the q factors 1, 0.85, 0.5 and 0.3, the relative ages and the initial carbon activity (Ao). M = Modern.

Bore ID	Formation	$\delta^{13}C$	a ¹⁴C (pMC)	q CH₄	q calc.	q sulph.	Age (q = 1)	Ao	Age (q = 0.85)	Ao	Age (q = 0.5)	Ao	Age (q = 0.3)	Ao
50876	Boisdale Formation	−13.2	26.11	0.85	0.85		11,101	26.11	9758	30.72	5371	52.22	1148	87.03
52753	Boisdale Formation	−2.4	16.52	0.51	0.85		14,886	16.52	13,542	19.44	9155	33.04	4932	55.07
52754	Latrobe Group	−6.2	19.53	0.63	0.85		13,502	19.53	12,158	22.98	7772	39.06	3549	65.10
58935	Latrobe Group	−2.3	17.43	0.51	0.85		14,442	17.43	13,099	20.51	8712	34.86	4489	58.10
58937	Latrobe Group	−12.4	51.14	0.82	0.85		5544	51.14	4200	60.16	M	102.28	M	170.47
61125	Older Volcanics	−18.4	76.05	1.00	0.85	0.99	2263	76.05	920	89.47	M	152.10	M	253.50
61184	Older Volcanics	−15.4	27.45	0.92	0.85		10,688	27.45	9344	32.29	4957	54.90	734	91.50
64835	Latrobe Valley Coal Measures	−0.8	46.19	0.46	0.85		6385	46.19	5042	54.34	655	92.38	M	153.97
76079	Latrobe Group	−17.0	24.24	0.97	0.85		11,716	24.24	10,372	28.52	5985	48.48	1762	80.80
77436	Latrobe Group	−18.9	16.05	1.00	0.85	0.98	15,124	16.05	13,781	18.88	9394	32.10	5171	53.50
86670	Boisdale Formation	−7.2	45.07	0.66	0.85		6588	45.07	5245	53.02	858	90.14	M	150.23
89809	Latrobe Group	−6.3	61.73	0.63	0.85		3988	61.73	2644	72.62	M	123.46	M	205.77
90149	Boisdale Formation	−5.8	20.45	0.62	0.85		13,121	20.45	11,778	24.06	7391	40.90	3168	68.17
90366	Latrobe Group	−7.3	1.04	0.67	0.85		37,747	1.04	36,403	1.22	32,016	2.08	27,793	3.47
92118	Latrobe Group	13.4	24.29	0.02	0.85		11,699	24.29	10,355	28.58	5968	48.58	1745	80.97
96560	Latrobe Group	−14.6	24.52	0.89	0.85		11,621	24.52	10,277	28.85	5891	49.04	1668	81.73
103811	Boisdale Formation	−15.9	103.34	0.93	0.85		M	103.34	M	121.58	M	206.68	M	344.47
105132	Boisdale Formation	6.3	50.44	0.24	0.85		5658	50.44	4314	59.34	M	100.88	M	168.13
105483	Latrobe Group	−5.8	47.46	0.62	0.85		6161	47.46	4818	55.84	431	94.92	M	158.20
105547	Boisdale Formation	−12.9	41.48	0.84	0.85		7275	41.48	5931	48.80	1544	82.96	M	138.27
107970	Older Volcanics	−15.2	17.83	0.91	0.85		14,255	17.83	12,911	20.98	8524	35.66	4301	59.43
107971	Childers Formation	−17.7	29.61	0.99	0.85		10,061	29.61	8718	34.84	4331	59.22	108	98.70
107972	Childers Formation	−12.7	1.02	0.84	0.85		37,907	1.02	36,564	1.20	32,177	2.04	27,954	3.40
110725	Latrobe Group	−11.2	22.73	0.79	0.85		12,247	22.73	10,904	26.74	6517	45.46	2294	75.77
110729	Latrobe Group	−20.3	23.51	1.00	0.85	0.95	11,969	23.51	10,625	27.66	6238	47.02	2015	78.37
143749	Haunted Hill	−13.4	104.43	0.86	0.85		M	104.43	M	122.86	M	208.86	M	348.10
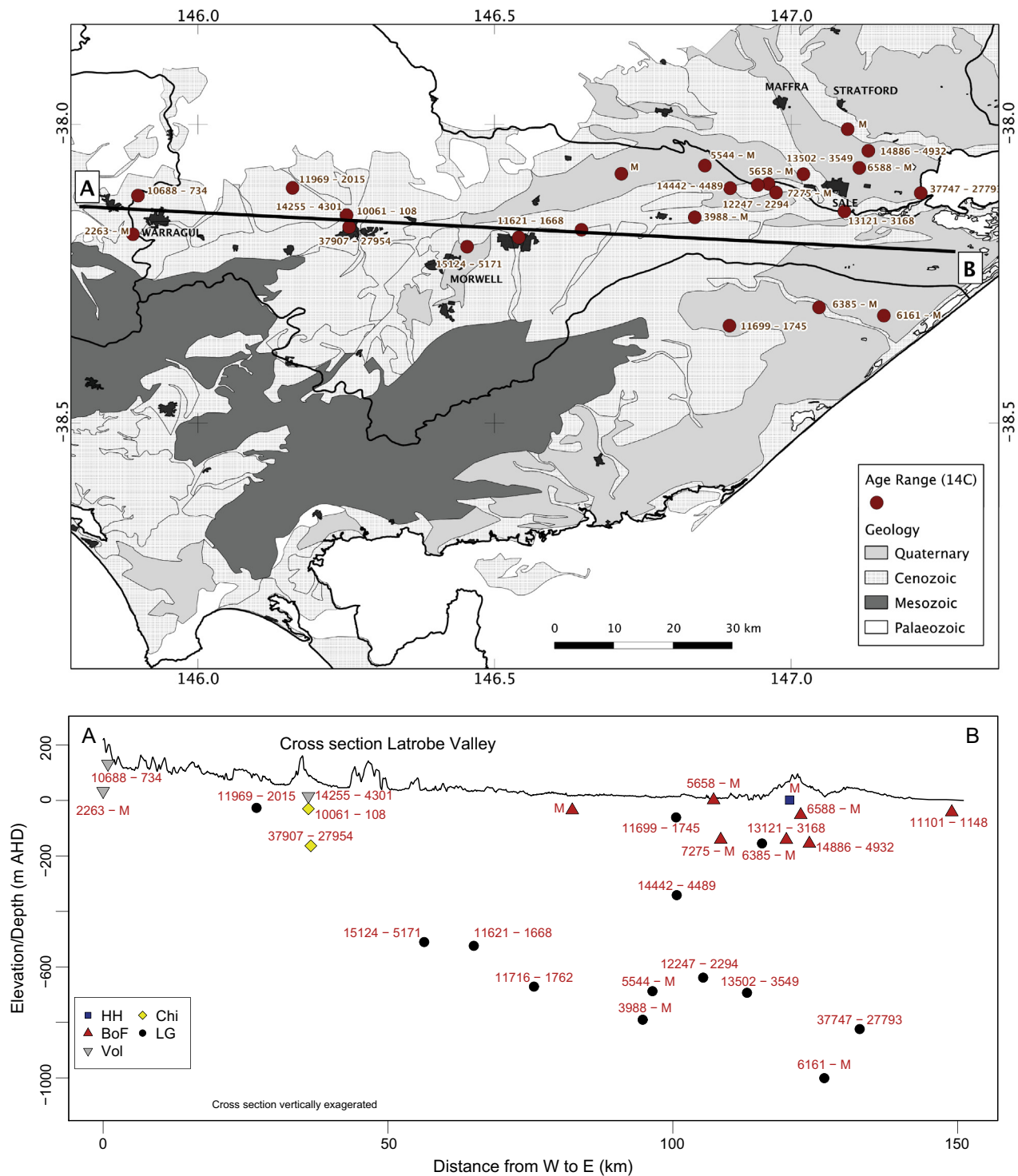
Fig. 11. Map and cross section showing the distribution of corrected C age ranges across the Latrobe Valley and with depth (Table 5). (Abbreviations: HH – Haunted Hill Formation, BoF – Boisdale Formation, Vol – Thorpdale Volcanics, Chi – Childers Formation, LG – Latrobe Group).

Values of q calculated assuming that $\delta^{13}C_r = -18$‰ are between 0.02 and 1, although most are in the range 0.5–0.8 (Table 5).

Sulfate reduction via Eq. (4) produces DIC with $\delta^{13}C$ values of the organic matter that is being oxidised. If it is assumed that SO_4 reduction is the predominant process in samples with $\delta^{13}C$ values lower than those of recharge, $q_{sulfate}$ values may be calculated using an analogous equation to Eq. (5). Again assuming that the organic matter has $\delta^{13}C$ values of -25‰ and recharge has $\delta^{13}C$ values of -18‰ yields q values of >0.95 for the samples in Table 5.

Given the multiplicity of processes, correcting the ^{14}C ages is subject to considerable uncertainty; however, it is possible to constrain the plausible range of values. Corrected ^{14}C ages (t) are given by:

$$t = -8376 \, \ln \left(\frac{a^{14}C}{q \cdot a_0{}^{14}C} \right) \tag{5}$$

Calculated q values are between 0.3 and 1 (Table 5) yielding ages between 37,907 ka and modern (i.e., where the groundwater contains a significant component of water recharged after the

atmospheric nuclear tests in the 1950s and 1960s). The following observations help place limits on the range of possible q values. Firstly, the groundwater is generally ^3H free except for samples 103,811 and 143,749; however, with $q = 0.5$ there are samples with calculated modern ^{14}C ages that are ^3H free, which is highly unlikely. In aquifers where significant methanogenesis has caused dilution of ^{14}C, groundwater with a^{14}C similar to those in the Latrobe Valley contains ^3H. Secondly, if groundwater is modern, its initial a^{14}C will be a$^{14}C/q$. Using the q values in Table 5, initial a^{14}C are up to 350 pMC, which are far higher than the maximum a^{14}C recorded in the soil zone ($\sim$120 pMC: Cook and Herczeg, 2000; Rethemeyer et al., 2005) or the atmosphere ($\sim$200 pMC: Suess, 1971; Clark and Fritz, 1997). Thus, whilst realising the uncertainty in the calculations, ^{14}C ages are calculated for $q = 0.5$–0.85, which covers the range estimated for calcite dissolution in silicate aquifers and the majority of the methanogenesis estimates.

Groundwater ages are up to 36 ka to modern and do not increase systematically along the flow paths within the aquifers (Fig. 11). Younger ages are found in the eastern part of the basin and at greater depth. The general downward hydraulic gradient in the western and central part of the basin transports younger water to deeper units, especially in the western part, while a reverse gradient occurs in some aquifers in the far eastern sections. This suggests that groundwater ages should increase with depth in the western and central areas and that the age gradient from shallow to deeper units declines towards the east. However, this is not reflected in the age distributions (Fig. 11). Hence, the regional distribution of heads does not reflect smaller scale preferential flow paths. Furthermore, the hydraulic gradients in the west alone cannot account entirely for the younger groundwater ages in deeper aquifers. Fault zones are likely to present preferential flow paths along which younger water reaches greater depth. The volcanic formations in the West are highly fractured, which would allow faster transport. Fractures allow constituents in the groundwater to move by advection, while dispersion and matrix diffusion are more dominant in very slowly moving parts of the aquifer with low hydraulic conductivities (Sanford, 1996). This can lead to large differences in ^{14}C ages. Also, leakage from lower conductivity lenses in the alluvial deposits and leakage from aquitards may influence the ages. Both processes enhance with increasing ages. Despite this being a problem and a possible correction is not likely to change the results significantly. The high variability of ^{14}C ages across the aquifers with depth in combination with the heterogeneous major ion chemistry suggests that inter-aquifer mixing occurs mainly along hydraulically active fracture zones.

4. Conclusions

In summary, the combination of major ion geochemistry, stable isotopes, and radiogenic isotopes allows a better understanding of groundwater flow paths and inter-aquifer mixing in the Gippsland Basin, which could not be derived from the analysis of hydraulic heads alone. Despite the difference in aquifer lithology and a relatively complex stratigraphy, there is little difference in the major ion geochemistry, stable isotope ratios, or $^{87}Sr/^{86}Sr$ ratios of groundwater within the basin. In similar large inter-mountain basins where groundwater mixing is limited, groundwater from the different aquifers commonly has contrasting major ion geochemistry (Ge and Garven, 1992; Garven, 1995; Tóth, 1995; Stuyfzand, 1999; Carrillo-Rivera et al., 2007; Fernandes et al., 2010). The high $\delta^{13}C$ values indicate that methanogenesis has occurred in parts of the Boisdale Formation and the Latrobe Group while $\delta^{34}S$ values indicates SO_4 reduction in parts of the Latrobe Group and the Childers Formation.

Carbon-14 ages also do not increase uniformly with distance from the catchment margins or with depth, which is also consistent with relatively complex flow paths and inter-aquifer mixing (Fig. 11). As discussed above, correction of the ^{14}C ages is difficult, however the distribution of a^{14}C is also irregular implying that this is not an artefact of the correction process. Inter-aquifer mixing is enhanced due to lateral connectivity in between aquifers where sediments interlace and the lack of aquitards within the basin. In addition, large hydraulically active faults such as those occurring within the Rosedale and Wonwron monoclines (Fig. 4) penetrate the Tertiary sediments.

The results of this study illustrate the use of hydrogeochemistry to constrain inter-aquifer-mixing in large basins with complex stratigraphy that are used for water resources. While groundwater extraction mostly occurs within the shallow Quaternary and younger Tertiary aquifers, the fact that the aquifers are hydraulically connected may increase gradients in between aquifers, which can result in depleting old groundwater resources that will not be recharged (Fig. 3). Furthermore, given the broad recharge area; groundwater is susceptible to contamination from agricultural activities, urban and industrial waste water. Shallow groundwater from the Haunted Hill Formation and the Boisdale Formation is connected to deeper units due to missing aquitards and possibly hydraulic fault systems, exposing not only the shallow units to contamination but also deeper units across the basin. Predicting where these impacts are most likely remains difficult due to the heterogeneous nature of the aquifer system in the Latrobe Valley. Currently, there is ample evidence for inter-aquifer mixing from the geochemistry. Groundwater flow paths have changed over time due to groundwater extraction. The extent to which groundwater extraction has influenced the degree of inter-aquifer mixing is not known as there is no historic geochemical data. This uncertainty illustrates the need to carry out baseline geochemical studies to properly characterise long term hydrogeological processes prior to resource development.

Acknowledgements

References

Alcala, J.F., Custodio, E., 2008. Using the Cl/Br ratio as a tracer to identify the origin of salinity in aquifers in Spain and Portugal. J. Hydrol. 359, 189–2007.

Aravena, R., Robertson, W.D., 1998. Use of multiple isotope tracers to evaluate denitrification in ground water: study of nitrate from a large-flux septic system plume. Ground Water 36, 975–982.

Aravena, R., Wassenaar, L.I., Plummer, L.N., 1995. Estimating ^{14}C groundwater ages in a methanogenic aquifer. Water Resour. Res. 31, 2307–2317.

Ayers, G.P., Ivey, J.P., 1988. Pricipitation composition at Cape Grim, 1977–1985. Tellus 40B, 297–307.

Ayraud, V., Aquilina, L., Labasque, T., Pauwels, H., Molenat, J., Pierson-Wickmann, A.-C., Durand, V., Bour, O., Tarits, C., Le Corre, P., Fourre, E., Merot, P., Davy, P., 2008. Compartmentalization of physical and chemical properties in hard-rock aquifers deduced from chemical and groundwater age analyses. Appl. Geochem. 23, 2686–2707.

Backburn, G., McLeod, S., 1983. Salinity of atmospheric precipitation in the Murray–Darling Drainage Division, Australia. Geochim. Cosmochim. Acta 21, 434–441.

Brumley, J., Barton, C., Holdgate, G., Reid, M., 1981. Regional groundwater investigation of the Latrobe Valley: 1976–1981. Tech. Rep., State Electricity Commission of Victoria Department of Minerals and Energy, Melbourne, Australia.

Carrillo-Rivera, J., Varsanyi, I., Kovacs, L., Cardona, A., 2007. Tracing groundwater flow systems with hydrogeochemistry in contrasting geological environments. Water Air Soil Pollut. 184, 77–103.

Cartwright, I., Weaver, T.R., Cendón, D.I., Fifield, L.K., Tweed, S.O., Petrides, B., Swane, I., in press. Constraining groundwater flow, residence times, inter-aquifer mixing, and aquifer properties using environmental isotopes in the southeast Murray Basin, Australia. Appl. Geochem. 27(9), 1698–1709.

Cartwright, I., Weaver, T., Cendón, D.I., Swane, I., 2010. Environmental isotopes as indicators of inter-aquifer mixing, Wimmera Region, Murray Basin, Southeast Australia. Chem. Geol. 277, 214–226.

Cartwright, I., Weaver, T.R., Fifield, L.K., 2006. Cl/Br ratios and environmental isotopes as indicators of recharge variability and groundwater flow: an example from the southeast Murray Basin, Australia. Chem. Geol. 231, 38–56.

Cartwright, I., Weaver, T.R., Fulton, S., Nichol, C., Reid, M., Cheng, X., 2004. Hydrogeochemical and isotopic constraints on the origins of dry land salinity, Murray Basin, Victoria, Australia. Appl. Geochem. 19, 1233–1254.

Cartwright, I., Weaver, T.R., Petrides, B., 2007a. Controls on $^{87}Sr/^{86}Sr$ ratios of groundwater in silicate-dominated aquifers: SE Murray Basin, Australia. Chem. Geol. 246, 107–123.

Cartwright, I., Weaver, T.R., Stone, D., Reid, M., 2007b. Constraining modern and historical recharge from bore hydrographs, H, C, and chloride concentrations: applications to dual-porosity aquifers in dry land salinity areas, Murray Basin, Australia. J. Hydrol. 332, 69–92.

Cerling, T.E., Pederson, B.L., Von-Damm, K.L., 1989. Sodium–calcium ion exchange in the weathering of shales: implications for global weathering budget. Geology 17, 552–554.

Clark, I.C., Fritz, P., 1997. Environmental Isotopes in Hydrogeology. Lewis Publishers.

Cochrane, G.W., Quick, G.W., Jones, S., 1991. Introducing Victorian Geology, first ed. Geological Society of Australia, Victorian Division, Melbourne.

Coetsiers, M., Walraevens, K., 2009. A new correction model for Cages in aquifers with complex geochemistry – application to the Neogene Aquifer, Belgium. Appl. Geochem. 24, 768–776.

Cook, P.G., Herczeg, A.L., 2000. Environmental Tracers in Subsurface Hydrogeology. Kluwer Academic Publishers.

Cook, P.G., Jolly, I.D., Leaney, F.W., Walker, G.R., Allan, G.L., Fifield, L.K., Allison, G.B., 1994. Unsaturated zone tritium and chlorine 36 profiles from southern Australia: their use as tracers of soil water movement. Water Resour. Res. 30, 1709–1719.

Coplen, T.B., 1988. Normalization of oxygen and hydrogen isotope data. Chem. Geol. 72, 293–397.

Davis, S.N., Whittemore, D.O., Fabryka-Martin, J., 1998. Use of chloride/bromide ratios in studies of potable water. Ground Water 36, 338–350.

Department of Sustainability and Environment (DSE), 2009. Gippsland Region Sustainable Water Strategy: Discussion Paper. Tech. Rep., Department of Sustainability and Environment.

Department of Sustainability and Environment (DSE), 2010. Report for ecoMarkets Groundwater Models: Groundwater Flow Modeling: West Gippsland CMA. Tech. Rep., Department of Sustainability and Environment.

Dogramaci, S.S., Herczeg, A.L., 2002. Strontium and carbon isotope constraints on carbonate-solution interactions and inter-aquifer mixing in groundwaters of the semi-arid Murray Basin, Australia. J. Hydrol. 262, 50–67.

Douglas, J., Ferguson, J., 1988. Geology of Victoria. Geological Society of Australia.

Downing, R., Edmunds, W., Gale, I., 1987. Regional groundwater flow in sedimentary basins in the UK. In: Goff, J.C., Williams, B.P.J. (Eds), Fluid Flow in Sedimentary Basins and Aquifers. Geological Society Special Publication 34, pp. 105–125.

Edmunds, W.E., 2009. Geochemistry's vital contribution to solving water resource problems. Appl. Geochem. 24, 1058–1073.

Emblanch, C., Zuppi, G., Mudry, J., Blavoux, B., Batiot, C., 2003. Carbon-13 of TDIC to quantify the role of the unsaturated zone: the example of the Vaucluse Karst System (Southern France). J. Hydrol. 279, 262–274.

Faure, G., Mensing, T.M., 2004. Isotopes: Principles and Applications, third ed. Wiley and Sons.

Fernandes, P., Carreira, P., Bahir, M., 2010. Mass balance simulation and principal components analysis applied to groundwater resources: Essaouira basin (morocco). Environ. Earth Sci. 59, 1475–1484.

Fogg, G.E., 1986. Groundwater flow and sand body interconnectedness in a thick, multiple-aquifer system. Water Resour. Res. 22, 679–694.

Fontes, J.-C., 1983. Dating of groundwater. In: Guidebook on Nuclear Techniques in Hydrology, Technical Reports Series No. 91. IAEA, Vienna.

Freeze, R.A., 1974. Streamflow generation. Rev. Geophys. 12, 627–647.

Fritz, S.J., Drimmie, J., Fritz, P., 1991. Characterizing shallow aquifers using tritium and ^{14}C: periodic sampling based on tritium half-life. Appl. Geochem. 6, 17–33.

Gallagher, S., Greenwood, D., Taylor, D., Smith, A., Wallace, M., Holdgate, G., 2003. The pliocene climatic and environmental evolution of South-Eastern Australia: evidence from the marine and terrestrial realm. Palaeogeog. Palaeoclimatol. 193, 349–382.

Garven, G., 1995. Continental-scale groundwater flow and geologic processes. Ann. Rev. Earth Planet Sci. 23, 89–117.

Ge, S., Garven, G., 1992. Hydromechanical modeling of tectonically driven groundwater flow with application to the arkoma foreland basin. J. Geophys. Res. 97, 9119–9144.

Gerritse, R.G., George, R.J., 1988. The role of soil organic matter in the geochemical cycling of chloride and bromide. J. Hydrol. 101, 83–95.

Gibson-Poole, C., Svendsen, L., Underschultz, J., Watson, M., Ennis-King, J., van Ruth, P., Nelson, E., Daniel, R., Cinar, Y., 2006. Gippsland Basin geosequestration: a potential solution for the Latrobe Valley brown coal CO_2 emissions. APPEA J..

Gibson-Poole, C., Svendsen, L., Underschultz, J., Watson, M., Ennis-King, J., Van Ruth, P., Nelson, E., Daniel, R., Cinar, Y., 2008. Site characterisation of a basin-scale CO_2 geological storage system: Gippsland Basin, southeast Australia. Environ. Geol. 54, 1583–1606.

Herczeg, A.L., Edmunds, W.M., 2000. Inorganic ions as tracers. In: Cook, P.G., Herczeg, A.L. (Eds.), Environmental Tracers in Subsurface Hydrogeology. Kluwer Academic Publishers.

Holdgate, G.R., McGowran, B., Fromhold, T., Wagstaff, B.E., Gallagher, S.J., Wallace, M.W., Sluiter, I.R., Whitelaw, M., 2009. Eocene-Miocene carbon-isotope and floral record from brown coal seams in the Gippsland Basin of southeast Australia. Global Planet. Change 65, 89–103.

Holdgate, G., Kershaw, A., Sluiter, I., 1995. Sequence stratigraphic analysis and the origins of Tertiary brown coal lithotypes, Latrobe Valley, Gippsland Basin, Australia. Int. J. Coal Geol. 28, 249–275.

Holdgate, G.R., Wallace, M., Gallagher, S., Smith, A.J., Keene, J.B., Moore, D., Shafik, S., 2003. Plio-Pleistocene tectonics and eustasy in the Gippsland Basin, southeast Australia: evidence from magnetic imagery and marine geolgcial data. Aust. J. Earth Sci. 50, 403–426.

Holdgate, G.R., Wallace, M.W., Gallagher, S.J., Taylor, D., 2000. A review of the Traralgon Formation in the Gippsland Basin – a world class brown coal resource. Int. J. Coal Geol. 45, 55–84.

Hoque, M.A., Burgess, W.G., 2012. ^{14}C dating of deep groundwater in the Bengal Aquifer System, Bangladesh: implications for aquifer anisotropy, recharge sources and sustainability. J. Hydrol. 444–445, 209–220.

Jencso, K.G., McGlynn, B.L., 2011. Hierarchical controls on runoff generation: topographically driven hydrologic connectivity, geology, and vegetation. Water Resour. Res. 47. http://dx.doi.org/10.1029/2011WR010666, W11527, 16.

Jones, J.G., Veevers, J.J., 1982. A Cainozoic history of Australia's Southeast Highlands. J. Geol. Soc. Aust. 29, 1–12.

Katz, B.G., Bullen, T.D., 1996. The combined use of $^{87}Sr/^{86}Sr$ and carbon and water isotopes to study hydrochemical interaction between groundwater and lake water in mantled karst. Geochim. Cosmochim. Acta 60, 5075–5087.

Koschorreck, M., Wendt-Potthoff, K., Scharf, B., Richnow, H.H., 2008. Methanogenesis in the sediment of the acidic Lake Cviahue in Argentina. J. Volcanol. Geotherm. Res. 178, 197–204.

Lakey, R., Tickell, S., 1981. Explanatory notes on the Western Port Groundwater Basin 1:100 000 Hydrogeological Map. Tech. Rep. 69, Geological Survey Report.

Leybourne, M., Clark, I., Goodfellow, W., 2006. Stable isotope geochemistry of ground and surface waters associated with undisturbed massive sulfide deposits: constraints on origin of waters and water-rock interactions. Chem. Geol. 231, 300–325.

Ma, J.Z., Wang, X.S., Edmunds, W.M., 2005. The characteristics of ground-water resources and their changes under the impacts of human activity in the arid northwest china—a case study of the shiyang river basin. J. Arid Environ. 61, 277–295.

Mahlknecht, J., Schneider, J.F., Merkel, B.J., de Léon, I.N., Bernasconi, S.M., 2004. Groundwater in a sedimentary basin in semi-arid Mexico. Hydrogeol. J. 12, 511–530.

Maloszewski, P., Zuber, A., 1991. Influence of matrix diffusion and exchange reactions on radiocarbon ages in fissured carbonate aquifers. Water Resour. Res. 7, 1937–1945.

Mazor, E., 2004. Chemical and Isotopic Groundwater Hydrology. Marcel Dekker, Inc..

McNutt, R.H., 2000. Strontium isotopes. In: Cook, P.G., Herczec, A.L. (Eds.), Environmental Tracers in Subsurface Hydrology. Kluwer Academic Publishers, Boston, pp. 233–260.

Mook, W.G., Bommerson, J.C., Staverman, W.H., 1974. Carbon isotope fractionation between dissolved bicarbonate and gaseous carbon dioxide. Earth Planet. Sci. Lett. 22, 169–176.

Nahm, G.Y., 2002. The Hydrogeology of the Gippsland Basin and its Role in the Genesis and Accumulation of Petroleum. Ph.D. Thesis, School of Earth Sciences, Univ. Melbourne.

Neklapilova, B., 2008a. Conductivity Measurements and Large Volumes Distillation of Samples for Tritium analysis. ANSTO internal guideline. Technical Report ENV-I-070-002, ANSTO – Institute for Environmental Research, Australia.

Neklapilova, B., 2008b. Electrolysis and Small Volume Distillation Of Samples For Tritium Activity Analysis, ANSTO internal guideline. Technical Report ENV-I-070-003, ANSTO – Institute for Environmental Research, Australia.

Norvick, M., Smith, M., Power, M., 2001. The plate tectonic evolution of eastern Australasia guided by the stratigraphy of the Gippsland Basin. In: Hill, K.C., Bernecker, T. (Eds), Eastern Australasian Basins Symp., Petroleum Exploration Society of Australia, Special Edition.

O'Sullivan, P., Mitchell, M., O'Sullivan, A., Kohn, B., Gleadow, A., 2000. Thermotectonic history of the Bassian Rise, Australia: implications for the breakup of eastern Gondwana along Australia's southeastern margins. Earth Planet. Sci. Lett. 182, 31–47.

Plummer, L.N., Sprinkle, C.L., 2001. Radiocarbon dating of dissolved inorganic carbon in groundwater from confined parts of the Upper Floridian aquifer, Florida, USA. Hydrogeol. J. 9, 127–150.

Quade, J., Chivas, A., McCulloch, M., 1995. Strontium and carbon isotope tracers and the origins of soil carbonate in South Australia and Victoria. Palaeogeog. Palaeoclimatol. Paloeoecol. 113, 103–117.

Rahmanian, V., Moore, P., Mudge, W., Spring, D., 1990. Sequence stratigraphy and the habitat of hydrocarbons, Gippsland Basin, Australia. In: Geological Society of London, Special Publication 50, 525–544.

Raiber, M., Webb, J.A., Bennetts, D.A., 2009. Strontium isotopes as tracers to delineate aquifer interactions and the influence of rainfall in the basalt plains of Southeastern Australia. J. Hydrol. 367, 188–199.

Rethemeyer, J., Kramer, C., Gleixner, G., John, B., Yamashita, T., Flessa, H., Andersen, N., Nadeau, M.-J., Grootes, P.M., 2005. Transformation of organic matter in agricultural soils: radiocarbon concentration versus soil depth. Geoderma 128, 94–105.

Ross, M., Parent, M., Lefebvre, R., 2005. 3D geologic framework models for regional hydrogeology and land-use management: a case study from a quaternary basin of South-Western Quebec, Canada. Hydrogeol. J. 13, 690–707.

Saliege, J.F., Fontes, J.C., 1984. Essai de détermination expérimentale du fractionnement des isotopes ^{13}C et ^{14}C du carbone au cours de processus naturels. Int. J. Appl. Radiat. Isot. 35, 55–62.

Sanford, W.E., 1996. Correction for diffusion in carbon-14 dating of ground water. Ground Water 35, 357–361.

Sayed, S.A.S., Saeedy, H.S., Szekely, F., 1992. Hydraulic parameters of a multi-layered aquifer system in Kuwait City. J. Hydrol. 130, 49–70.

Schaeffer, J., 2008. Scaling Point Based Aquifer Data for Developing Regional Groundwater Models. Ph.D. Thesis, Univ. Melbourne.

Southern Rural Water, 2009. Hydrogeological Mapping of Southern Victoria. Tech. Rep., Southern Rural Water.

Strapoc, D., Mastalerz, M., Dawson, K., Macalady, J., Callaghan, A.V., Wawrik, B., Turich, C., Ashby, M., 2011. Biogeochemistry of Microbial Coal-Bed Methane. Ann. Rev. Earth. Planet. Sci. 39, 617–656.

Stuiver, M., Polach, A., 1977. Reporting of C data. Radiocarbon 19, 355–363.

Stuyfzand, P.J., 1999. Patterns in groundwater chemistry resulting from groundwater flow. Hydrogeol. J. 7, 15–27.

Suess, H.E., 1971. Climatic changes and the amtosheric radiocarbon level. Palaeogeog. Palaeoclimatol. Paloeoecol. 10, 199–201.

Thompson, B., 1986. The Gippsland Basin – development and stratigraphy. In: Glenie R.C. (Ed.), Second south-eastern Australia Oil Symp. (Melbourne, Australia, 1986), Petroleum Exploration Society of Australia, Victorian and Tasmanian Branch.

Tosolini, A.-M.P., McLoughlin, S., Drinnan, A., 1999. Stratigraphy and fluvial sedimantary facies of the Neocomian lower Strzelecki Group, Gippland Basin, Victoria. Aust. J. Earth Sci. 46, 951–970.

Tóth, J., 1995. Hydraulic continuity in large sedimentary basins. Hydrogeol. J. 3, 4–16.

Valentine, D.L., Chidthaisong, A., Rice, A., Reeburgh, W.S., Tyler, S.C., 2004. Carbon and hydrogen isotope fractionation by moderately thermophilic methanogens. Geochim. Cosmochim. Acta 68, 1571–1590.

Van der Kemp, W., 2000. Inverse chemical modeling and radiocarbon dating of palaeoground waters: the Tertiary Ledo-Paniselian aquifer in Flanders, Belgium. Water Resour. Res. 36, 1277–1287.

Varma, S., Michael, K., 2011. Impact of multi-purpose aquifer utilisation on a variable-density groundwater flow system in the Gippsland Basin, Australia. Hydrogeol. J. 20, 119–134.

Victorian Water Warehouse, 2011. Department of Sustainability and Environment Data Warehouse. <http://www.vicwaterdata.net/vicwaterdata/home.aspx>.

Walker G., Mollica, F., 1990. Review of the Groundwater Resources in the South East Region. Technical Report 54, Department of Water Resources Victoria.

Webb, J.A., Gardner, T.W., Kapostasy, D., Bremar, K.A., Fabel, D., 2011. Mountain building along a passive margin: late Neogen tectonism in southeastern Victroia, Australia. Geomorphology 125, 253–262.

Whiticar, M., Farber, E., Schoell, M., 1986. Biogenic methane formation in marine and freshwater environments: CO_2 reduction vs. acetate fermentation – Isotope evidence. Geochim. Cosmochim. Acta 50, 693–709.

Willcox, J., Sayers, J., 2001. Gower Basin, Lord Howe Rise. Petrol. Explor. Soc. Aust. Special Publication 1, 189–200.

Zuber, A., Witczak, S., Rózański, K., Śliwka, I., Opaka, M., Mochalski, P., Kuc, T., Karlikowska, J., Kania, J., Jackowicz-Korczyński, M., Duliński, M., 2005. Groundwater dating with ^{3}H and SF_6 in relation to mixing patterns, transport modelling and hydrochemistry. Hydrolog. Process. 19, 2247–2275.